Aerosol size distribution and new particle formation in western Yangtze River Delta of China: two-year measurement at the SORPES station

X. M. Qi[1,3], A. J. Ding[1,3,*], W. Nie[1,3], T. Petäjä[2], V.-M. Kerminen[2], E. Herrmann[1,**], Y. N. Xie[1], L. F. Zheng[1,3], H. Manninen[2], P. Aalto[2], J. N. Sun[1,3], Z. N. Xu[1,3], X.G. Chi[1,3], X. Huang[1,3], M. Boy[2,3], A. Virkkula[1,2,3], X.-Q. Yang[1,3], C.B. Fu[1,3], and M. Kulmala[2]

[1]Institute for Climate and Global Change Research & School of Atmospheric Sciences, Nanjing University, 210023, Nanjing, China

[2]Department of Physics, University of Helsinki, 00014 Helsinki, Finland

[3]Collaborative Innovation Center of Climate Change, Nanjing, Jiangsu Province, China

[*]Correspondence to A.J. Ding (dingaj@nju.edu.cn)

** Now at Laboratory for Atmospheric Chemistry, Paul Scherrer Institute, Switzerland

Abstract:

Aerosol particles play important roles in regional air quality and global climate change. In this study, we analyzed two-year (2011-2013) measurement of submicron particles (6-800 nm) at a suburban site in western Yangtze River delta (YRD) of East China. The number concentrations (NCs) of particles in the nucleation, Aitken and accumulation modes were 5300 ± 5500 cm^{-3}, 8000 ± 4400 cm^{-3}, 5800 ± 3200 cm^{-3}, respectively. The NCs of total particles are comparable to that at urban/suburban sites in other Chinese megacities, such as Beijing, but about 10 times higher than the remote western China. Long-range and regional transports influenced largely on number concentrations and size distributions of submicron particles. The highest and lowest accumulation mode particle number concentrations were observed in air masses from YRD and coastal region, respectively. Continental air masses from inland brought the highest concentrations of nucleation mode particles. New particle formation (NPF) events, apparent in 44% of the effective measurement days, occurred frequently in all the seasons except winter. The frequency of NPF in spring, summer and autumn is much higher than other measurement sites in China. Sulfuric acid

was found to be the main driver of NPF events. The particle formation rate was the highest in spring (3.6 ±2.4 cm^{-3} s^{-1}), whereas the particle growth rate had the highest values in summer (12.8 ± 4.4 nm h^{-1}). The formation rate was typically high in relatively clean air masses, whereas the growth rate tended to be high in the polluted YRD air masses. The frequency of NPF events and the particle growth rates showed a strong year-to-year difference. In the summer of 2013, associated with a multi-week heat wave and strong photochemical processes, NPF events occurred with larger frequency and higher growth rates comparing with the same period in 2012. The difference in the location and strength of sub-tropical high pressure system, which influences the air mass transport pathways and solar radiation, seems to be the cause for year-to-year differences. This study reported, up to now, the longest continuous measurement records of submicron particles in East China and gained a comprehensive understanding of the main factors controlling the seasonal and year-to-year variation of the aerosol size distribution and NPF in East China.

1. Introduction

Atmospheric aerosols affect human life by influencing both air quality and climate (e.g. Charlson et al., 1992; Menon et al., 2002; Akimoto, 2003; Heal et al., 2012; IPCC, 2013). Fine particles, especially the submicron ones, have received lots of attention due to their close connection to climate via light extinction (Malm et al., 1994), cloud droplet activation (Kerminen et al., 2005; Wiedensohler et al., 2009; Sihto et al., 2011) and precipitation formation (Gettelman et al., 2013; Lebo and Feingold, 2014), as well as due to their adverse effects on human health (Pope et al., 2002; Rao et al., 2012).

Numerous studies have been conducted all over the world focusing on the characters of submicron particles, including their chemical composition and size distribution as well as their formation and growth in the atmosphere (e.g. Woo et al., 2001; Birmili et al., 2003; Engler et al., 2007; Zhang et al., 2007; Dal Maso et al., 2008; Laakso et al., 2008; Jimenez et al.,2009; Komppula et al., 2009; Asmi et al., 2011; Kerminen et al., 2012; Vakkari et al.,2013;Kulmala et al., 2014; Nie et al., 2014; Nieminen et al., 2014). In China, studies on submicron particles started about a decade ago. However, to the best of our knowledge, there are only three studies in China providing more than 1-year measurement of aerosol size distributions, with two of them conducted in North China Plain (Wu et al., 2007; Shen et al., 2011) and one at Mount Waliguan in remote western China (Kivekäs et al., 2009). Therefore, knowledge about the temporal variation of submicron particles and their relationship to meteorology and human activities in China is rather poor, even in some well-developed regions such as Yangtze River Delta (YRD) in East China.

The YRD has experienced rapid urbanization and industrialization in the last two decades, which have induced large amounts of fossil fuel consumption in the region and resulted in serious air pollution (Chameides et al., 2002; Ding et al., 2013ab; Tie and Cao, 2009; Li et al., 2011). In addition, YRD is a region influenced by typical Asian monsoon, which dominates the temporal and spatial variations of particles (Qian et al., 2003; Ding et al., 2013a). However, previous studies on aerosols in this region were mainly on mass concentrations and chemical compositions (e.g. Huang et al., 2012; Cheng et al., 2013; Ding et al., 2013a); studies on the number concentrations and size distributions were rather limited. In Nanjing, Herrmann et al. (2014) reported the first

result of about 4-month data of aerosol size distribution at the SORPES station, a suburban site in Nanjing, and Wang et al. (2014) reported about one month data at another suburban site. Both studies were conducted during the cold season. In other regions of the YRD, Gao et al. (2009) reported an intensive campaign in the early summer of 2005 in Taicang, a small town nearby Shanghai, and Du et al. (2011) reported winter time measurements from October 2008 to February 2009 in Shanghai. These results showed significant differences in both the diurnal patterns and NPF characteristics between the two seasons, and emphasize the need of continuous long-term measurements on the number size distributions of submicron particles in this region.

In the present study, we report two-year continuous observation of submicron particles (6-800 nm) and related quantities (including trace gases, $PM_{2.5}$ mass concentration and meteorological data) recorded at the SORPES (Station for Observing Regional Processes of the Earth System) site in suburban Nanjing of western YRD from December 2011 to November 2013. The aim of this work is to characterize the temporal variations of particle number size distributions and occurrence of new particle formation (NPF) in the western part of YRD, and to improve our understanding on the sources and processes influencing the atmospheric aerosol population in the developed region in China.

2. Experiment and Methodology

2.1Site information and measurements

This study was conducted at the SORPES station (Station for Observation Regional Process of the Earth System) developed in 2011 (Ding et al., 2013a). The site is located about 20 km northeast of downtown Nanjing (118°57'10''E, 32° 07'14''N, 40 m above ground level). With few local sources within 2-3 km surround, it can be considered as a regional background site in the well-developed YRD of East China. More details of the site, including trace gas, $PM_{2.5}$ and meteorological measurements, can be found in Ding et al. (2013a).

Size distribution of submicron particles is measured with a DMPS (Differential Mobility Particle Sizer) constructed at the University of Helsinki in Finland. This instrument was also involved in the instrument inter-comparison workshops conducted within the European

infrastructure project EUSAAR (European Supersites for Atmospheric Aerosol Research) and ACTRIS (Aerosols, Clouds, and Trace gases Research Infrastructure Network) (Wiedensohler et al., 2012). Before entering the inlet of the instrument, the particles are cut off at 2.5 μm and then dried (using Nafion tube from December 2011 to June 2012 and silica gel dryer after June 2012). The instrument consists of one DMA (Differential Mobility Analyzer) in different flow rates and one CPC (Condensation Particle Counter, TSI Model 3772). The DMA segregates the particles into exact narrow size ranges based on different narrow ranges of electrical mobility of charged particles in the electrical field. Equilibrium charge is ensured by two Americium 241 sources (each about 37 kBq) before particles enter the DMA. The DMPS is a flow-switching type differential mobility particle sizer in which two different sample and sheath air flow rates for the DMA are used to cover a wide size range. In the high flow mode, the sample air and sheath air flows are 3 and 20 L min^{-1}, respectively, and in the low flow mode they are 1 and 5 L min^{-1}, respectively. The high flow mode measures the size from 6 to 100 nm and the low flow mode measures from 100 to 800 nm. The measurement time interval of the instrument is 10 minutes during which the total particle number concentration is measured by CPC directly and 29 channels (16 for low flow rate and 13 for high flow rate) are scanned. Weekly maintenance, including flow rate adjusting and impactor cleaning, is routinely performed. The data assimilation in two flow modes and the test of data quality are described in the Appendix.

2.2 Calculation of variables characterizing new particle formation

The calculation of particle growth and formation rates along with the condensation sink were made following the procedure described by Kulmala et al. (2012). The growth rate (GR) of particles during the NPF events can be expressed as:

$$\mathrm{GR} = \frac{\mathrm{d}d_\mathrm{p}}{\mathrm{d}t} = \frac{\Delta d_\mathrm{p}}{\Delta t} = \frac{d_{\mathrm{p}2} - d_{\mathrm{p}1}}{t_2 - t_1} \quad (1)$$

where $d_{\mathrm{p}1}$ and $d_{\mathrm{p}2}$ are the representative of the diameter of nucleated particles at the times t_1 and t_2, respectively. For calculation, $d_{\mathrm{p}1}$ and $d_{\mathrm{p}2}$ are defined as the centre of size bin and t_1 and t_2 are the times when the concentration of this size bin reaches the maximum.

The formation rate of particles of diameter d_p is obtained from:

$$J_{\mathrm{d_p}} = \frac{\mathrm{d}N_{d_\mathrm{p}}}{\mathrm{d}t} + \mathrm{CoagS}_{d_\mathrm{p}} \times \mathrm{N}_{d_\mathrm{p}} + \frac{\mathrm{GR}}{\Delta d_\mathrm{p}} \times \mathrm{N}_{d_\mathrm{p}} + \mathrm{S}_{\mathrm{losses}} \quad (2)$$

where the first term on the right side is the time evolution of the particle number concentration in the size range $[d_{\mathrm{p}}, d_{\mathrm{p}} + \Delta d_{\mathrm{p}}]$. The second term is the coagulation loss approximated by the product of coagulation sink ($\mathrm{CoagS}_{d_{\mathrm{p}}}$) and the number concentration in the size range $[d_{\mathrm{p}}, d_{\mathrm{p}} + \Delta d_{\mathrm{p}}]$. The third term is the growth out of the considered size range where GR is the observed growth rate. The fourth term represents additional losses which were not considered in this study.

Having positive correlation with the coagulation sink (CoagS), the condensation sink (CS) describes the speed at which condensable vapour molecules condense onto the existing aerosol. It is expressed as:

$$\mathrm{CS} = 4\pi \int_0^{d_{\mathrm{p}}\max} \beta_{\mathrm{m}}\left(d'_{\mathrm{p}}\right) d'_{\mathrm{p}} \mathrm{N}_{d'_{\mathrm{p}}} \mathrm{d}d'_{\mathrm{p}} = 4\pi D \sum_{d'_{\mathrm{p}}} \beta_{\mathrm{m},d'_{\mathrm{p}}} d'_{\mathrm{p}} N_{d'_{\mathrm{p}}}, \tag{3}$$

where D is the diffusion coefficient of the condensing vapour, β_{m} is a transition-regime correction, d'_{p} is the discrete diameter and $\mathrm{N}_{d'_{\mathrm{p}}}$ is the particle number concentration in respective size bin. The increase of CS due to the particle hygroscopic growth was also estimated. The hygroscopic growth factor (GF), i.e. the ratio of the particle diameter at an ambient relative humidity (RH) to the corresponding "dry" particle diameter, was determined using the method described by Laakso et al. (2004),

$$\mathrm{GF} = \left(1 - \frac{\mathrm{RH}}{100}\right)^{\gamma(\mathrm{d_p})} \tag{4}$$

Here $\gamma(\mathrm{d_p})$ depends on the particle diameter ($\mathrm{d_p}$) and was obtained by a least square fit to hygroscopicity data. As there were no measured hygroscopic growth data at the SORPES station, the hygroscopicity data from another site in north of downtown Nanjing (Wu et al., 2014) was used.

Sulfuric acid has been identified as the main factor of new particle formation (Kulmala et al., 2013). Therefore, in this study we used the semi-empirical equation constructed by Mikkonen et al. (2011) to calculate the sulfuric acid proxy,

$$[\mathrm{H_2SO_4}] = 1.30 \times 10^{-1} \cdot \mathrm{k} \cdot \mathrm{Radiation}^{1.10} \cdot [\mathrm{SO_2}]^{0.69} \cdot \mathrm{CS}^{-0.53} \cdot \mathrm{RH}^{-1.92} \tag{5}$$

where *k* is the reaction rate constant.

3. Results and discussions

3.1 Particle number concentrations and size distributions

3.1.1 Overall results

Figure 1a shows the averaged particle number size distribution during the studied period. It shows a typical multimodal distribution as a result of combination of three lognormal distributions in the nucleation (6-30 nm), Aitken (30-100 nm) and accumulation modes (100-800 nm). Figure 1b illustrates the average fraction of the particle number, surface and volume concentration in these three modes. It shows features similar to most other continental regions in the lower troposphere, i.e. the nucleation and Aitken mode particles (<100 nm) dominate the number concentration, and accumulation mode particles control the surface and volume concentration (Raes et al., 2000; Asmi et al., 2011).

As shown in Table 1, the average total particle number concentration (NC) over the diameter range 6-800 nm during the two-year period was 19200 ± 9200 cm^{-3}, with the values of 5300 ± 5500 cm^{-3} in the nucleation mode (6-30 nm), 8000 ± 4400 cm^{-3} in the Aitken mode (30-100 nm) and 5800 ± 3200 cm^{-3} in the accumulation mode (100-800 nm), respectively. The NC of total particle at SORPES in Nanjing are comparable to those measured at the urban site (about 32700 cm^{-3} in the size range of 3-1000 nm) (Wu et al., 2008) and at a rural site in Beijing (about 11500 cm^{-3} in the size range of 3-1000 nm) (Shen et al., 2011), while about 10 times higher than those measured at Mount Waliguan, a remote background site in western China (about 2100 cm^{-3} in the size range of 12-570 nm) (Kivekäs et al., 2009). One typical feature at SORPES is the high concentration of accumulation mode particles, which can be up to several times the typical concentrations measured in Europe or North America (200 to 2900 cm^{-3} compared to 5700 cm^{-3} at SORPES in the size range of 100-500 nm) (Stanier et al., 2004; Asmi et al., 2011; Wang et al., 2011).

3.1.2 Seasonal variations

The average seasonal variations of particle number concentrations during the two-year measurements are presented in Fig. 2. Nucleation mode particles had highest concentrations in winter (December to January) and spring (April). Aitken mode particles showed similar patterns with an additional peak in July. Accumulation mode particles showed high concentrations in January and June and low concentrations in July, which is similar to the seasonal variation of

$PM_{2.5}$ concentration reported by Ding et al. (2013a). As accounting for almost 70% of the total particles, the nucleation and Aitken mode particles dominated the seasonal cycle of the total particle number concentration. The exact values and standard deviations of the particle number concentrations in spring (March - May), summer (June - August), autumn (September - November) and winter (December - February) are given in Table 1. Seasonally, the nucleation and Aitken mode particles showed the highest concentrations in spring (6200 cm^{-3} ± 5900 cm^{-3} and 8500 cm^{-3} ± 4000 cm^{-3}, respectively), whereas highest concentrations of accumulation mode particles were observed in winter (6500 cm^{-3} ± 3000 cm^{-3}). The arithmetic mean diameter (AMD) of the particles and condensation sink (CS) revealed also seasonal cycles (Table 1), with the highest values observed in winter ($AMD_{6\text{-}800\ nm}$: 97 nm ± 26 nm, CS_{dry}: 4.2×10^{-2} s^{-1} ± 1.9×10^{-2} s^{-1}, CS: 5.8×10^{-2} s^{-1} ±2.7×10^{-2} s^{-1}). Given that the hygroscopicity measurements was conducted at another site in Nanjing (Wu et al., 2014), the hygroscopic growth associated with the calculation of CS at SORPES station might have large uncertainties. We therefore deployed the CS without considering the hygroscopic growth in the following discussion.

Generally, the seasonal patterns of NC of submicron particles at SORPES were related to the long-range transport associated with the Asian monsoon climate and also anthropogenic emissions. Figure 3 presents the seasonal variations of four meteorological variables (temperature, pressure, radiation and rainfall) during the two-year measurement period. In winter, few rains and low boundary layer favor the accumulation of pollutants and result in high particle loadings. Besides, the winter heating in northern China would bring aged accumulation mode particles to Nanjing via the regional transports (Zhang et al., 2009; Li et al., 2011). In summer, the dominantly rainy and unstable weather (e.g. convection and monsoon precipitation) leads to low particle number concentrations, especially for accumulation mode particles. Radiation, which drives NPF events, influences the NCs of nucleation and Aitken mode particles. Moreover, an evident holiday effect can also influence the observed temporal variation. For example, the low particle loadings in all the modes can be identified in February (see Fig. 2) when Chinese have the winter break to celebrate the Spring Festival (Ding et al., 2013a).

Biomass burning (BB) is an important source of accumulation mode particles in early summer (Ding et al., 2013a and 2013b), so the burning of wheat straw in northern and middle part

of East China (Wu et al., 2008; Shen et al., 2010) is the plausible cause for the observed particle NCs peak in June (Fig. 2d). Here, we defined BB events as potassium concentration K^+>2 μg cm^{-3} and $K^+/PM_{2.5}$ ratio > 0.02 (K^+ was measured using MARGA, Nie et al., 2015). The average NC of accumulation mode particles during BB events in June was 31700 cm^{-3}, which is almost 6 times higher than the corresponding NC in non-BB event days (5300 cm^{-3}). Relatively large (>100 nm) particles are emitted directly from BB (Reid et al., 2005; Li et al., 2007), or formed rapidly after emissions by the combination of NPF and various particle growth processes (Hennigan et al., 2012; Vakkari et al., 2014). Such particles are able to promote atmospheric heterogeneous chemistry by providing a large surface area (Nie et al., 2015), influence the global climate by enhancing the CCN capacity (Hennigan et al., 2012), and even change the everyday weather (Ding et al., 2013b).

3.1.3 Diurnal pattern in different seasons

The diurnal cycles of particle number size distributions had similar patterns in spring, summer and autumn, which were connected to the events of new particle formation and growth, showing the typical 'banana' shape during daytime (Fig. 4a-4c). However, obvious differences could be observed for the starting time and strength of NPF in different seasons. It needs to be pointed out that in the averaged diurnal pattern in spring, summer and autumn (Fig. 4a-4c) the NPF had a relatively low number concentration of 6-15 nm particles, which is different from a typical NPF event. The main reason for this feature is that the averaged patterns include both event and non-event days and that sub-100 nm particle tend to grow also during non-event days without a clear formation of new sub-15 nm particles. A detailed discussion on NPF events will be given in section 3.2. Compared with other seasons, the high peaks of NC around 20-30nm and 100 nm during the wintertime rush hours in the morning and late afternoon (Fig.4d) suggest that local combustion sources, such as vehicle emission, played a more important role in the diurnal cycle of the total particle concentration than sources like regional NPF and growth.

In order to investigate the detailed diurnal variations of the particle NCs in different modes, we compared the diurnal patterns of the three modes in seasons: spring and winter (Fig. 5a-5c). For nucleation mode particles, peak concentrations appeared at noontime in spring but at the early morning or later afternoon in winter. The later suggests a possible influence from human activities, such as vehicle emissions under conditions of a low mixing layer. For the Aitken mode particles,

in spring the highest concentrations were seen about two hours after the appearance of the peak in the nucleation mode, which was due to the growth of nucleated particles to larger sizes (Fig.5b). In winter, Aitken mode particles had peaks at the same time or a bit later than what the nucleation mode particle did. The diurnal variation of the accumulation mode particle number concentration (Fig. 5c) was controlled by the development of the boundary layer in both seasons, having a pattern similar to that of the $PM_{2.5}$ concentration (Ding et al., 2013a).

3.1.4 The influences of air masses

Figure 6 shows backward trajectory cluster analysis for the SORPES site. Using the Hybrid Single-Particle Lagrangian Integrated Trajectory (HYSPLIT) model Version 4.9 (Draxler and Hess, 1998) driven with Global Data Assimilation System (GDAS) output, 5 clusters of trajectories were identified based on hourly 3-day backward trajectories for the period of December 2011-November 2013. Here we calculated the trajectories for 3 days by considering a rough turnover time of about 2.4 days for 200 nm particles (Tunved et al., 2005). The results showed that air masses arriving at the SORPES site generally came from the inland continent (14.8% of the air masses belonging to the cluster C2 and 13.0% to the cluster C3), coastal North China (C1: 30.6%, C4 and C5 together: 41.6% in total). The two continental air masses had distinguished source regions, with C2 passed over the North China Plain and C3 traveled over a large are of BVOCs. For the coastal air messes, C5 was much local compared to C4, but the latter just crossed the city-cluster along Nanjing-Shanghai axis and might have an additional marine signature. The air mass transport pattern was controlled by Asian monsoon (Ding et al., 2013a), with winter monsoon bringing regional pollution from the North China Plain (C2, C1 and C5) and summer monsoon bringing the YRD regional pollution (C4) or biogenic emissions from the South China to the site (C3). Being located in the most western part of the YRD, SORPES is a unique site to investigate the impact of different regional air masses.

The average behavior of the particles number size distributions and diurnal variations of NCs in the three modes in the five air mass clusters are shown in Fig. 7. The coastal air masses (C1) had the lowest accumulation mode particle loading during the whole day (Fig. 7d). The continental air masses (C2 and C3) had highest levels of nucleation mode particles (Fig. 7b), probably associated with the dry and sunny weather. Since C3 air masses occurred mostly in

summer and travelled over regions abundant in BVOCs emissions, these air masses preferred NPF and resulted in the highest concentrations of nucleation mode Aitken mode particles (Fig. 7b, c). The YRD air masses (C4 and C5), passing through the YRD city clusters, brought the highest accumulation mode particle loadings (Fig.7d) and lowered concentrations of nucleation mode particles (Fig. 7b) due to the high coagulation/condensation sinks. C5 air masses, with more locally air and less influences of marine air, displayed larger concentrations of accumulation mode particles and lower concentrations of Aitken mode particles (Fig 7c, d).

3.2 New particle formation (NPF)

3.2.1 Population statistic about NPF

The sampling days during the 2-year measurements were classified into NPF event days, non-event days and undefined days with the criterion whether a nucleation burst occurred or not. By following the method used by Dal Maso et. al. (2005) and Kulmala et al. (2012), the event days were further classified into Class I when the formation and growth rate can be calculated with confidence, and Class II when the formation and growth rate cannot be calculated or done in accurate ways.

The numbers of the four types of sampling days are given in Table 2, and the percentages of them in each month are shown in Fig. 8a. Due to instrument maintenance, data from 111 days of the two-year period were unavailable for the event classification. Only few of the days at SORPES were considered as undefined days (11 days), for which it was hard to determine whether a NPF event occurred or not. Overall, NPF event days (including Class I and Class II days) accounted for 44% of the sampling days. This frequency is a bit higher than observed in the other two long-term measurements in China (urban Beijing ~40%, SDZ ~37%). In spring, summer and autumn, NPF events took place in about half of the sampling days (55%, 54% and 49%, respectively), which is more frequent than at other measurement sites in China, including as Taicang (44%), Hong Kong (34%) and Xinken (26%) (Gao et al., 2008; Guo et al., 2012; Liu et al., 2008). A higher frequency of NPF events in the warm season is similar to what has been observed in most other sites all over the world and is mainly because of higher radiation and stronger biogenic activity during that time of the year (Manninen et al., 2010). In contrast, in winter only 15 NPF event days during two-year

measurement period were identified. This frequency is similar to another work in Shanghai (Du et. al., 2012), but quite different from that in Beijing where winter is the second season favorable to NPF (Wu et al., 2007; Shen et al., 2011). One explanation for this could be that there are more 'clean' days in winter in Beijing because of frequent cold fronts (Wehner et al., 2008). In June, continuous rainy days ('plum rain' in China) with low radiation also inhibit the NPF events. There was a great difference in the frequency of NPF events in summer between the two years: 39% in 2012 and 66% in 2013 (Fig. 8a).

Figure 8b gives the variability of start and end times of the Class I event days. Since the cut-off diameter of the DMPS was 6 nm, the start and end times were defined here as the times when the 6-7 nm particles started to increase and decrease back to the background level (i.e. ~ 50 cm^{-3}). Generally, the start time was somewhere between the sunrise and midday, and no evident nocturnal events were identified. The seasonal variation of the start time followed that of sunrise, which is similar to reported elsewhere around the world (e.g. Woo et al., 2001; Boy and Kulmala et al., 2002; Kulmala et al., 2004; Hamed et al., 2007; Wu et al., 2007). However, at some days the start time was just one hour after the sunrise. Most of such events took place in summer and were associated with marine air masses that had been transported over the polluted area in YRD. This topic will be studied further in our future work.

The formation rate of 6-nm particles (J_6) and growth rate of 6 to 30 nm particles ($GR_{6\text{-}30\ nm}$) during the Class I event days are illustrated in Fig. 8c and 8d. The statistical results are given in Table 2. The formation rates were highest in spring with the value of 3.6 $\pm$2.4 cm^{-3} s^{-1}, followed by summer (2.1 $\pm$1.4 cm^{-3} s^{-1}) and autumn (2.1 $\pm$1.9 cm^{-3} s^{-1}), whereas the lowest formation rates were observed in winter (1.8 $\pm$1.6 cm^{-3} s^{-1}). The maximum formation rate was 10.9 cm^{-3} s^{-1} on 3 April, 2013. The observed formation rates in Nanjing are comparable to other measurements in China, e.g. 3.3-81.4 cm^{-3} s^{-1} in Beijing (for J_3), 0.7-72.7 cm^{-3} s^{-1} with mean value 8 cm^{-3} s^{-1} at SDZ (for J_3), 3.4 cm^{-3} s^{-1} (3 October - 5 November, 2004) in PRD (for J_3), 3.8 cm^{-3} s^{-1} (25 October – 29 November, 2010) in Hong Kong (for $J_{5.5}$ on Class I days), and about 2.2 cm^{-3} s^{-1} (5 May – 2 June, 2005) in Shanghai (for J_{10}) (Wu et al., 2007; Shen et al., 2011; Liu et al., 2008; Guo et al., 2012; Gao et al., 2008). Concerning the nuclei growth rates, the highest values of 12.8 $\pm$4.4 nm h^{-1} were observed in summer, followed by spring (10.0 $\pm$3.4 nm h^{-1}), winter (9.5 $\pm$3.3 nm h^{-1}) and autumn

(8.9 ± 2.9 nm h^{-1}). The maximum growth rate was 22.9 nm h^{-1}, observed on 29 August, 2013. The values of growth rates presented in this study for Nanjing are slightly higher than reported for the other two long-term measurements in China, i.e. 0.1-11.2 nm h^{-1} in Beijing and 0.3-14.5 nm h^{-1} with mean value of 4.3 nm h^{-1} at SDZ (Wu et al., 2007; Shen et al., 2011).

3.2.2 Conditions favoring NPF

In Figure 9, we compare the NPF related parameters between the event (Class I and Class II) and non-event days in different seasons. As shown in Fig. 9a and 9b, higher temperatures and lower RH favored the NPF events. Having a higher temperature on event days is similar to observations made in Germany and Italy (Birmili and Wiednsohler, 2000; Birmili et al., 2003; Hamed et al., 2007), but different from observations made in Finland or in the tropopause region (Boy and Kulmala, 2002; Hamed et al., 2007; Young et al., 2007). A lower RH on event days is similar to what has been observed in most of boundary layer stations (Boy and Kulmala, 2002; Birmili et al., 2003; Hamed et al., 2007; Guo et al., 2012). In general, a low RH is related to sunny days with strong radiation, which favor the formation of OH (Hamed et al., 2007). In addition, a low RH will decrease the condensation sink by slowing the hygroscopic growth (Hamed et al., 2011).

Radiation and O_3 concentrations were higher on event days than those on non-event days (Fig. 9c, d), indicating that the observed NPF events in YRD were typically photochemically influenced. In line with most boundary layer stations (Manninen et al., 2010), lower $PM_{2.5}$ concentrations and CS favored the occurrence of NPF events (Fig. 9e, g). On average, higher SO_2 concentrations were observed on event days in spring and summer, while the events in autumn and winter favored lower SO_2 concentrations (Fig. 9f). This result was in accordance with our previous study conducted in winter time that suggested NPF to occur preferably under conditions of lower SO_2 concentrations (Herrmann et al., 2014). In autumn and winter, the SO_2 peaks were always accompanied with a high $PM_{2.5}$ concentration in YRD. Therefore, the observed lower SO_2 concentrations on event days in autumn and winter are understandable as the pre-existing particles play a more important role. The proxy of H_2SO_4 was significantly higher on event days than on non-event days, suggesting the sulfuric acid was the main driver of NPF events at SORPES.

The statistics of the NPF events in different air masses clusters are given in Table 3. The events influenced by two or more air mass groups, which were about 17% of sampling days, were not included in this statistic. Air masses in C3 revealed the most frequent NPF (54 event days and 12 non-event days). As illustrated in section 3.1.4, C3 air masses took place usually in summer and brought large amounts of BVOCs (e.g. monoterpenes) from south China (Fig. 6a). BVOC emissions have previously been observed to contribute to the formation and growth of new particles (Birmili et al., 2003; Tunved et al., 2006; Fu and Kawamura, 2011; Kamens et al., 2011). Air masses in C4 and C5, which passed through polluted YRD area with lots of pre-existing particles, generally had less NPF events, further indicating that the polluted YRD plume would suppress the formation of new particles. In winter, when solar radiation is low, no NPF events occurred in the YRD area masses (Herrmann et al., 2014).

3.2.3 Factors influencing particle formation and growth rates

To investigate the factors that influence the formation rate and growth rate, the correlation coefficients of J_6 and $GR_{6\text{-}30nm}$ with meteorological quantities and gaseous pollutants were calculated (Table 4). The correlation coefficients that passed the statistical significance test ($p<0.05$) were highlighted by asterisk in Table 4.The particle formation rate (J_6) was negatively correlated with RH and positively correlated with both radiation and O_3. No significant correlation between J_6 and SO_2 was seen at SORPES. The particle growth rate was positively correlated with temperature, RH, radiation, O_3 and CS ($p<0.05$).Worth noting here is that while lower values of RH and CS appeared to favor the occurrence of a NPF event, higher values of these two quantities clearly favored the particle growth. This suggests that the new formation and growth are influenced, at least to some extent, by different processes and vapors (Yli-Juuti et al., 2011; Rose et al., 2015). The scatter plots of J_6-RH and $GR_{6\text{-}30\ nm}$-RH color-coded with O_3 mixing ratio are shown in Fig. 10. The negative correlation between J_6 and RH did not depend on the O_3 concentration (Fig. 10a), whereas for $GR_{6\text{-}30\ nm}$ an obvious difference in the $GR_{6\text{-}30\ nm}$-RH slope could be identified for different levels of the O_3 mixing ratio (Fig. 10b). Here the good GR-RH relationship may also be influenced by factors other than the O_3 mixing ratio, such as the transport compounds acting as precursors for the vapors responsible for the particle growth. Because of the influence of summer monsoon, air masses from the southeast and southwest directions are

generally much humid than those from the north. These southerly air masses could also be accompanied with high concentration of BVOCs or anthropogenic VOCs and their oxidants. Ding et al. (2013a) found that air masses from the YRD city clusters were always associated with high concentration of O_3, which should also contain high concentration of anthropogenic VOCs.

In order to study further the event with high or low value of $J_6/GR_{6\text{-}30nm}$, we conducted Lagrangian dispersion modeling for the selected days marked in Fig. 8c and 8d, by using the method developed by Ding et al.(2013c) based on HYSPLIT model to study the influence of air masses. Fig. 11 gives the footprint, i.e. retroplume at an altitude of 100 m, of the selected high and low $J_6/GR_{6\text{-}30nm}$ days. Air masses had an obvious influence on the formation rate and growth rate. Most low J_6 days and high GR days occurred in the air masses passing over the polluted YRD area, while all the high J_6 days and low GR days appeared in air masses that did not go through the YRD area. This further suggests the differences in the particle formation and growth processes could partly explain the positive correlation between the GR and RH. In addition to the high RH in YRD air masses, the high anthropogenic VOCs concentration may play a more important role in enhancing the particle growth. Our finding that the polluted YRD plume induces a high GR is consistent with the studies reporting relatively high particle growth rates under urban conditions (Kulmala and Kerminen, 2008; Peng et al., 2014).

3.3 Causes on the high frequency of NPF in August 2013

As shown in Fig. 8, a higher frequency of NPF events occurred in July and August of 2013 compared with the same months in 2012. In August of 2013, the frequency of Class I NPF events was highest during the two-year measurement period, with 17 Class I events observed among the 24 analyzed days. Fig. 12 shows the time series of particle number size distribution, O_3 and $PM_{2.5}$ concentrations and radiation. The daily-average O_3 concentration gradually increased in early August with an hourly maximum value up to 165 ppbv on 12 August, 2013. Accompanied with this O_3 episode, the geometric mean diameter (GMD) of submicron particles and $PM_{2.5}$ concentration also increased (Fig 12a, b). Interestingly, there were continuously multi-day NPF events in the first half of this month, even during 11-13 August when $PM_{2.5}$ reached 70-80 μg m^{-3}. During 17-24 August, there were also notable NPF events. Contrary to this, few NPF took place in August 2012.

Examination of average geopotential height and wind vector at the 925-hPa level during the two Augusts(Fig. 13a) suggests that in 2013 the subtropical(Pacific) High moved more to the west than that in 2012, causing a positive anomaly (high pressure) and anti-cyclone over Southeast China (Fig. 13b). As a result, the Yangtze River Delta experienced a continuous heat wave with humid and hot air transported from the south and southwest.

In order to further understand the air masses history during the events in 2013, Fig. 14 gives the averaged "footprint" (i.e., 100 m retroplume) for the episode period. The air masses can be divided into three time periods. During 6-11 August, the air masses came from the southwest with high value of BVOCs and they also passed through the downtown of Nanjing. During this period, O_3 was produced and accumulated with enough precursors and strong solar radiation. High O_3 concentrations also caused a strong atmospheric oxidation capacity, which caused an increase in the GMD of submicron particles together with an increase in the$PM_{2.5}$ mass concentration. On 11 August, the air masses transport pathway was changed, with air masses coming mainly from southeast and the YRD city cluster, which is the most polluted area with high value of anthropogenic VOCs and other pollution gases. Therefore, the O_3concentration continued to increase until12 August and then maintained a high level until 19 August. A common character of the air masses during both of these two periods was that the air had transported over regions with high biogenic and anthropogenic emissions (See Figs. 6a, b and 14). During 19 to 22 August, the air masses were mainly from northeast and had a high humidity that caused cloudy days with low radiation and high wet deposition. The O_3 concentration, GMD of submicron particles and $PM_{2.5}$ mass concentration therefore sharply decreased on 19 August.

Despite the high levels of GMD, $PM_{2.5}$ and CS (which is not shown in Fig 12), Class I NPF events occurred every day during the whole O_3 episode (from 4 to 19 August, 2013). As the GMD and $PM_{2.5}$ increased, the particle formation rates became lower. This means that the high values of GMD and $PM_{2.5}$suppressed new particle formation but could not stop the occurrence of NPF event altogether under such an atmospheric condition of a high oxidization capacity. Because of lower pre-existing particle loading after 19 August, new particle formation continued although the radiation intensity and atmospheric ozone oxidation capacity were lower. Another obvious character for the August 2013 was that, during the whole month, the particle growth rate had a

relatively high correlation with RH (with r=0.54), supporting the positive correlation between GR and RH illustrated above (Fig. 15).

Here the year-to-year difference in aerosol size distributions and NPF characteristics suggests that large-scale circulations together with meteorological factors had a strong impact on the aerosol number concentration. Extreme meteorological conditions are able to reshape the seasonal profile of the aerosol number concentration and NPF, which means that measurements in a specific year cannot gain a full picture of seasonal profiles. Given the fact that there are only a limited number of measurements covering more than one year, especially in China, this work highlights the importance of long-term continuous measurement.

4. Summary

This study reports a two-year measurement (from December 2011 to November 2013) period of submicron particles (6-800 nm) at the SORPES station located in suburban Nanjing in the western part of YRD, East China, with the aim to characterize the temporal variation of the particle number concentration and size distribution, and to understand the new particle formation occurring in such a polluted monsoon area.

The average total number concentrations was 19200 ± 9200 (mean ± standard deviation) cm^{-3}, with 5300± 5500 cm^{-3} in the nucleation mode (6-30 nm), 8000±4400 cm^{-3}in the Aitken mode (30-100 nm) and 5800±3200 cm^{-3} in the accumulation mode (100-800 nm). Seasonal variations of NC and size distribution were influenced by the Asian monsoon, anthropogenic activities and atmospheric oxidation capacity. The diurnal pattern of the particle number size distribution in winter showed peaks at the normal rush hours, suggesting the source from direct emissions of vehicles. Air mass long-range transportation played clear roles in influencing the particle number concentration: coastal air masses had lowest concentrations of accumulation mode particles but relatively high concentrations of nucleation mode particles, continental air masses had the highest concentrations of nucleation mode particles with frequent new particle formation, and YRD air masses had the highest concentrations of accumulation mode particles and

lowest concentration of nucleation mode particles because of the elevated coagulation/condensation sinks.

NPF events were observed on 44% of the analyzed days, with the highest frequency in spring, followed by summer and autumn, but only 15 event days in winter. The average formation rates of 6 nm particles were 3.6±2.4, 2.1±1.4, 2.1±1.9 and 1.8±1.6 cm^{-3} s^{-1} in spring, summer, autumn and winter, respectively, and the corresponding particle growth rates were 10.0±3.4, 12.8±4.4, 8.9±2.9 and 9.5±3.3nm h^{-1}. A higher temperature, radiation intensity and O_3 concentration together with a lower RH and $PM_{2.5}$/CS ratio seemed to favor the occurrence of new particle formation events. Sulfuric acid appeared to play a key role in NPF event at SORPES. Trajectory analysis suggested that BVOC chemistry contributed to the new particle formation and growth. The particle formation rate was negatively correlated with RH and positively correlated with radiation and O_3 while particle growth rate was positively correlated with temperature, RH, radiation, O_3 and CS. Both particle formation and growth rate depended on the air mass origin, with low J_6 and high GR typical for polluted YRD air masses and high J_6 and low GR for clean air masses.

The observed frequency of NPF events and particle growth rate in summer showed a strong year-to-year variation under the influence of different large-scale circulations, such as subtropical High. Long-range transport, meteorological parameters and photochemical pollutants promoted the atmospheric new particle formation and growth in the summer 2013 compared with the previous year. To quantitatively understand the processes controlling the aerosol number concentration and size distribution, or to predict their behavior, additional modeling work on NPF that relies on long-term observations should be conducted in the future.

Acknowledgments. This work was supported by the National Natural Science Foundation of China (D0512/41305123 and D03/41321062). The SORPES-NJU stations were supported by the ’985 Program. Part of this work was supported by the Jiangsu Provincial Science Fund for Distinguished Young Scholars awarded to A.J. Ding (No. BK20140021) and by the Academy of Finland projects (1118615, 139656) and the European Commission via ERC Advanced Grant ATM-NUCLE.

Reference

Akimoto, H.: Global air quality and pollution, Science, 302, 1716-1719, doi:10.1126/science.1092666, 2003.

Asmi, A., Wiedensohler, A., Laj, P., Fjaeraa, A.M., Sellegri, K., Birmili, W., Weingartner, E., Baltensperger, U., Zdimal, V., Zikova, N., Putaud, J.P., Marinoni, A., Tunved, P., Hansson, H.C., Fiebig, M., Kivekas, N., Lihavainen H., Asmi, E., Ulevicius, V., Aalto, P.P., Swietlicki, E., Kristensson, A., Mihalopoulos, N., Kalivitis, N., Kalapov, I., Kiss, G., de Leeuw, G., Henzing, B., Harrison, R.M., Beddows, D., O'Dowd, C., Jennings, S.G., Flentje, H., Weinhold, K., Meinhardt, F., Ries, L., and Kulmala, M.: Number size distributions and seasonality of submicron particles in Europe 2008-2009, Atmos. Chem. Phys., 11, 5505-5538, doi:10.5194/acp-11-5505-2011, 2011.

Birmili, W., Berresheim, H., Plass-Dulmer, C., Elste, T., Gilge, S., Wiedensohler, A., andUhrner, U.: The Hohenpeissenberg aerosol formation experiment (HAFEX): a long-term study including size-resolved aerosol, H2SO4, OH, and monoterpenes measurement, Atmos. Chem. Phys., 3, 361-376, 2003.

Birmili, W. and Wiedensohler, A.: New particls formation in the continental boundary layer: Meteorological and gas phase parameter influence, Geophys. Res. Lett., 27, 3325-3328,doi:10.1029/1999gl011221, 2000.

Boy, M., and Kulmala, M.: Nucleation events in the continental boundary layer: Influence of physical and meteorological parameters, Atmos. Chem. Phys., 2,1-16, 2002.

Chameides, W.L., Luo, C., Saylor, R., Streets, D., Huang, Y., Bergin, M., and Giorgi, F.: Correlation between model-calculated anthropogenic aerosols and satellite-derived cloud optical depths: Indication of indirect effect?, J. Geophys. Res., 107, 4085,doi:10.1029/2000JD000208, 2002.

Charlson, R.J., Schwartz, S.E., Hales, J.M., Cess, R.D., Coakley Jr., J.A., Hansen, J.E., and Hofmann, D.J.: Climate forcing by anthropogenic aerosols, Science, 255, 423-430, doi: 10.1126/science.255.5043.423,1992.

Cheng, Z., Wang, S.X., Jiang, J.K., Fu, Q.Y., Chen, C.H., Xu, B.Y., Yu, J.Q., Fu, X.,andHao, J.M.: Long-term trend of haze pollution and impact of particulate matter in the Yangtze River Delta, China, Environ. Pollut., 182, 101-110, doi:10.1016/j.envpol.2013.06.043,2013.

Clarke, A. D., Varner, J. L., Eisele, F., Mauldin, R. L., Tanner, D. and Litchy, M.: Particle production in the remote marine atmosphere: Cloud outflow and subsidence during ACE 1, J. Geophys. Res. Atmospheres, 103(D13), 16397-16409, doi:10.1029/97JD02987, 1998.

Dal Maso, M., Kulmala, M., Riipinen, I., Wagner, R., Hussein, T., Aalto, P.P., and Lehtinen, K. E. J.: Formation and growth of fresh atmospheric aerosols: eight years of aerosol size distribution data from SMEAR II, Hyytiälä, Finland, Boreal Envron.Res., 10,323-336, 2005.

Dal Maso, M., Hyvärinen, A., Komppula, M., Tunved, P.,Kerminen, V.-M., Lihavainen, H., Viisanen, Y., Hansson, H.-C., and Kulmala, M.: Annual and interannual variation in boreal forest aerosol particle number and volume concentration and their connection to particle formation, Tellus, 60, 495-508, doi:10.1111/j.1600-0889.2008.00366.x,2008.

Ding, A. J., Fu, C. B., Yang, X. Q., Sun, J. N., Zheng, L. F., Xie, Y. N., Herrmann, E., Nie, W., Petäjä, T., Kerminen, V.-M., and Kulmala, M.: Ozone and fine particle in the western Yangtze River Delta: an overview of 1 yr data at the SORPES station, Atmos. Chem. Phys., 13,

5813-5830, doi:10.5194/acp-13-5813-2013,2013a.

Ding, A.J., Fu, C.B., Yang, X.Q., Sun. J.N., Petäjä, T., Kerminen, V.-M., Wang, T., Xie, Y., Herrmann, E., Zheng, L.F., Nie, W., Liu, Q., Wei, X.L.,andKulmala, M.: Intense atmospheric pollution modifies weather: a case of mixed biomass burning with fossil fuel combustion pollution in eastern China, Atmos. Chem. Phys., 13, 10545-10554, doi:10.5194/acp-13-10545-2013, 2013b.

Ding, A.J., Wang, T., and Fu, C.B.: Transport characteristics and origins of carbon monoxide and ozone in Hong Kong, South China, J. Geophys. Res., 118, 9475-9488, doi:10.1002/jgrd.50714, 2013c.

Draxler, R. R., and Hess, G. D.: An overview of the HYSPLIT 4 modeling system for trajectories dispersion and deposition, Aust. Meteoro. Mag., 47, 295–308, 1998.

Du, J.F., Cheng, T.T., Zhang, M., Chem, J.M., He, Q.S., Wang, X.M., Zhang, R.J., Tao, J., Huang, G.H., Li, X.,andZha, S.P.: Aerosol Size Spectra and Particle Formation Events at Urban Shanghai in Eastern China, Aerosol Air Qual. Res., 12, 1362-1372, doi:10.4209/aaqr.2011.12.0230,2012.

Engler, C., Rose, D., Wehner, B., Wiedensohler, A., Brüggemann, E., Gnauk, T., spindler, G., Tuch, T., andBirmili, W.: Size distribution of non-volatile particle residuals (Dp<800nm) at a rural site in Germany and relation to air mass origin, Atmos. Chem. Phys., 7, 5785-5802, doi:10.5194/acp-7-5785-2007,2007.

Fu, P. Q., and Kawamura, K.:Diurnal variations of polar organic tracers in summer forest aerosols: a case study of a Quercus and Picea mixed forest in Hokkaido, Japan, Geochem. J., 45, 297-308, 2011

Gao, J., Wang T., Zhou, X. H., Wu, W. S., and Wang, W. X.: Measure of aerosol number size distributions in the Yangtze River delta in China: Formation and growth of particles under polluted conditions, Atmos. Environ., 43, 829-836, doi:10.1016/j.atmosenv.2008.10.046, 2009.

Gettelman, A., Morrison, H., Terai, C. R., and Wood, R.: Microphysical process rates and global aerosol-cloud interactions, Atmos. Chem. Phys., 13, 9855-9867, doi:10.5194/acp-14-9099-2014, 2013.

Guo, H., Wang, D. W., Cheung, K., Ling, Z. H., Chan, C. K., and Yao X. H.: Observation of aerosol size distribution and new particle formation at a mountain site in subtropical Hong Kong, Atmos. Chem. Phys., 12, 9923-9939, doi:10.5194/acp-12-9923-2012,2012.

Hamed, A., Joutsensaari, J., Mikkonen, S., Sogacheva, L., Dal Maso, M., Kulmala, M., Cavalli, F., Fuzzi, S., Facchini, M.C., Decesari, S., Mircea, M., Lehtinen, K.E.J., andLaaksonen, A.: Nucleation and growth of new particles in Po Valley, Italy, Atmos. Chem. Phys., 7, 355-376, 2007.

Hamed, A., Korhonen, H., Sihto, S. L., Joutsensaari, J., Jarvinen, H., Petaja, T., Arnold, F., Nieminen, T., Kulmala, M., Smith, J. N., Lehtinen, K. E. J. and Laaksonen, A.: The role of relative humidity in continental new particle formation, J. Geophys. Res., 116, D03202, doi:10.1029/2010JD014186, 2011.

Heal, M. R., Kumar, P., and Harrison, R. M.: Particles, air quality, policy and health, Chem. Soc. Rev., 41, 6606-6630, doi:10.1039/C2CS35076A, 2012.

Hennigan, C. J., Westervelt, D. M., Riipinen, I., Engelhart, G. J., Lee, T.,Collett Jr., J. L., Pandis, S. N., Adams, P. J., and Robinson, A. L.: New particle formation and growth in biomass burning plumes: An important source of cloud condensation nuclei, Geophys. Res. Lett., 39, L09805,

doi:10.1029/2012gl050930, 2012.

Herrmann, E., Ding, A.J., Kerminen, V.-M., Petäjä, T., Yang, X.Q., Sun, J.N., Qi, X.M., Manninen, H., Hakala, J., Nieminen, T., Aalto, P.P., Kulmala, M., and Fu, C.B.: Aerosols and nucleation in eastern China: first insights from the new SORPES-NJU station, Atmos. Chem. Phys., 14, 2169-2183, doi:10.5194/acp-14-2169-2014, 2014.

Huang, X. F., He, L.Y., Xue, L., Sun, T.L., Zheng, L.W., Gong, Z.H., Hu, M., and Zhu, T.: Highly time-resolved chemical characterization of atmospheric fine particles during 2010 Shanghai World Expo, Atmos. Chem. Phys., 12,4897-4907, doi:10.5194/acp-12-4897-2012, 2012.

IPCC: Climate Change 2013: The Physical Science Basis. Contribution of Working Group I to the Fifth Assessment Report of the Intergovernmental Panel on Climate Change, edited by: Stocker, T. F., Qin, D., Plattner, G.-K., Tignor, M., Allen, S. K., Boschung, J., Nauels, A., Xia, Y., Bex, V., and Midgley, P. M., Cambridge University Press, Cambridge, United Kingdom and New York, NY, USA, 1535 pp, doi:10.1017/CBO9781107415324, 2013.

Jimenez, J. L., Canagaratna, M.R., Donahue, N.M., Prevot, A.S.H., Zhang, Q., Kroll, J.H., DeCarlo, P.F., Allan, J.D., Coe, H., Ng, N.L., Aiken, A.C., Docherty, K.S., Ulbrich, I.M., Grieshop, A.P., Robinson, A.L., Duplissy, J., Smith, J.D., Wilson, K.R., Lanz, V.A., Hueglin, C., Sun, Y.L., Tian, J., Laaksonen, A., Raatikainen, T., Rautiainen, J., Vaattovaara, P., Ehn, M., Kulmala, M., Tomlinson, J.M., Collins, D.R., Cubison, M.J., Dunlea, E.J., Huffman, J.A., Onasch, T.B., Alfarra, M.R., Williams, P.I., Bower, K., Kondo, Y., Schneider, J., Drewnick, F., Borrmann, S., Weimer, S., Demerjian, K., Salcedo, D., Cottrell, L., Griffin, R., Takami, A., Miyoshi, T., Hatakeyama, S., Shimono, A., Sun, J.Y., Zhang, Y.M., Dzepina, K., Kimmel, J.R., Sueper, D., Jayne, J.T., Herndon, S.C., Trimborn, A.M., Williams, L.R., Wood, E.C., Middlebrook, A.M., Kolb, C.E., Baltensperger, U., and Worsnop, D.R.: Evolution of organic aerosols in the atmosphere, Science, 326, 1525-1529, doi:10.1126/science.1180353,2009.

Kamens, R. M., Zhang, H. F., Chen, E. H., Zhou, Y., Parikh, H. M., Wilson, R. L., Galloway, K. E. and Rosen, E. P.: Secondary organic aerosol formation from toluene in an atmospheric hydrocarbon mixture: Water and particle seed effects, Atmos. Environ., 45, 2324-2334, doi: 10.1016/j.atmosenv.2010.11.007, 2011.

Kerminen, V.-M., Lihavainen, H., Komppula, M., Viisanen, Y.,andKulmala, M.: Direct observational evidence linking atmospheric aerosol formation and cloud droplet activation, Geophys. Res.Lett.,32, L14803, doi:10.1029/2005gl023130, 2005.

Kerminen, V.-M., Paramonov, M., Anttila, T., Riipinen, I., Fountoukis, C., Korhonen, H., Asmi, E., Laakso, L.,Lihavainen, H., Swietlicki, E., Svenningsson, B., Asmi, A.,Pandis, S.N., Kulmala, M., and Petäjä, T.: Cloud condensation nuclei production associated with atmospheric nucleation: a synthesis based on existing literature and new results, Atmos. Chem. Phys., 12, 12037-12059, doi:10.5194/acp-12-12037-2012, 2012.

Kivekäs, N., Sun, J., Zhan, M., Kerminen, V.-M., Hyvärinen, A., Komppula, M., Viisanen, Y., Hong, N., Zhang, Y., Kulmala, M., Zhang, X.-C., Deli-Geer, and Lihavainen, H.: Long term particle size distribution measurements at Mount Waliguan, a high altitude site in inland China, Atmos. Chem. Phys., 9, 5461-5474, 2009.

Komppula, M., Lihavainen, H., Hyvarinen, A.P., Kerminen, V.-M., Panwar, T.S., Sharma, V.P., andVisanen, Y.: Physical properties of aerosol particles at a Himalayan background site in India,J.Geophys. Res., 114, D12202, doi:10.1029/2008jd011007, 2009.

Kulmala, M., andKerminen, V.-M.: On the formation and growth of atmospheric nanoparticles,

Atmos. Res., 90, 132-150, doi:10.1016/j.atmosres.2008.01.005,2008.

Kulmala, M., Vehkamaki, H., Petäjä, T., Dal Maso, M., Lauri, A., Kerminen, V.-M., Birmili, W., and McMurry, P.H.: Formation and growth rates of ultrafine atmospheric particles: a review of observations, J. Aerosol Sci., 35, 143-176, doi:10.1016/j.jaerosci.2003.10.003,2004.

Kulmala, M., Petäjä, T., Nieminen, T., Sipilä, M., Manninen, H. E., Lehtipalo, K., Dal Maso, M., Aalto, P. P., Junninen, H., Paasonen, P., Riipinen, I., Lehtinen, K. E. J., Laaksonen, A., and Kerminen, V.-M.: Measurement of the nucleation of atmospheric aerosol particles, Nat. Protoc., 7, 1651-1667, doi:10.1038/nprot.2012.091,2012.

Kulmala, M., Kontkanen, J., Junninen, H., Lehtipalo, K., Manninen, H.E., Nieminen, T., Petäjä, T., Sipila, M., Schobesberger, S., Rantala, P., Franchin, A., Jokinen, T., Jarvinen, E., Aijala, M., Kangasluoma, J., Hakala, J., Aalto, P.P., Paasonen, P., Mikkila, J., Vanhanen, J., Aalto, J., Hakola, H., Makkonen, U., Ruuskanen, T., Mauldin, R.L., Duplissy, J., Vehkamaki, H., Back, J.,Kortelainen, A., Riipinen, I., Kurten, T., Johnston, M.V., Smith, J.N., Ehn, M., Mentel, T.F., Lehtinen, K.E.J., Laaksonen, A., Kerminen, V.-M., and Worsnop, D.R.: Direct Observation of Atmospheric Aerosol Nucleation, Science, 339, 943-946, doi:10.1126/science.1227385, 2013.

Kulmala, M., Petäjä, T., Ehn, M., Thornton, J., Sipilä, M., Worsnop, D. R., and Kerminen, V.-M.: Chemistry of atmospheric nucleation: On the recent advances on precursor characterization and atmospheric cluster composition in connection with atmospheric particle formation, Annu. Rev. Phys. Chem., 65, 21-37, doi:10.1146/annurev-physchem-040412-110014, 2014.

Laakso, L., Laakso, H., Aalto, P.P., Keronen, P., Petäjä, T., Nieminen, T., Pohja, T., Siivola, E., Kulmala, M., Kgabi, N., Molefe, M., Mabaso, D., Phalatse, D., Pienaar, K.,andKerminen, V.M.: Basic characteristics of atmospheric particles, trace gases and meteorology in a relatively clean Southern African Savannah environment, Atmos. Chem. Phys., 8, 4823-4839, 2008.

Lebo, Z. J., and Feingold G.: On the relationship between responses in cloud water and precipitation to changes in aerosol, Atmos. Chem. Phys., 14, 11817-11831, doi:10.5194/acp-14-11817-2014, 2014.

Li, L., Chen, C.H., Fu, J.S., Huang, C., Streets, D.G., Huang, H.Y., Zhang, G.F., Wang, Y.J., Jiang, C.J., Wang ,H.L., Chen, Y. R., and Fu, J.M.: Air quality and emissions in the Yangtze River Delta, China, Atmos. Chem. Phys., 11, 1621-1639, doi:10.5194/acp-11-1621-2011, 2011.

Li, X.H., Duan, L., Wang, S.X., Duan, J.C., Guo, X.M., Yi, H.H., Hu, J.N., Li, C., and Hao, J.M.: Emission characteristics of particulate matter from rural household biofuel combustion in China, Energy Fuels, 21, 845-851, doi:10.1021/ef060150g, 2007.

Liu, S., Hu, M., Wu Z. J., Wehner, B., Wiedensohler, A., and Cheng, Y. F.: Aerosol number size distribution and new particle formation at a rural/ coastal site in Pearl River Delta (PRD) of China, Atmos. Environ., 42, 6275-6283, doi:10.1016/j.atmosenv.2008.01.063, 2008.

Malm, W.C., Sisler, J.F., Huffman, D., Eldred, R.A., and Cahill, T.A.: Spatial and seasonal trends in particle concentration and optical extinction in the United-States, J. Geophys. Res., 99,1347-1370, doi:10.1029/93jd02916,1994.

Manninen, H. E., Nieminen, T., Asmi, E., Gagne, S., Hakkinen, S., Lehtipalo, K., Aalto, P., Vana, M., Mirme, A., Mirme, S., Horrak, U., Plass-Dulmer, C., Stange, G., Kiss, G., Hoffer, A., Torő, N., Moerman, M., Henzing, B., de Leeuw, G., Brinkenberg, M., Kouvarakis, G. N., Bougiatioti, A., Mihalopoulos, N., O'Dowd, C., Ceburnis, D., Arneth, A., Svenningsson, B., Swietlicki, E., Tarozzi, L., Decesari, S., Facchini, M. C., Birmili, W., Sonntag, A., Wiedensohler, A., Boulon, J., Sellegri, K., Laj, P., Gysel, M., Bukowiecki, N., Weingartner, E., Wehrle, G., Laaksonen, A.,

Hamed, A., Joutsensaari, J., Petaja, T., Kerminen, V.-M. and Kulmala, M.: EUCAARI ion spectrometer measurements at 12 European sites - analysis of new particle formation events, Atmos Chem Phys, 10(16), 7907-7927, doi:10.5194/acp-10-7907-2010, 2010.

McMurry, P. H., Fink, M., Sakurai, H., Stolzenburg, M. R., Mauldin, R. L., Smith, J., Eisele, F., Moore, K., Sjostedt, S., Tanner, D., Huey, L. G., Nowak, J. B., Edgerton, E., and Voisin, D.: A criterion for new particle formation in the sulfur-rich Atlanta atmosphere, J. Geophys. Res., 110, D22S02, doi:10.1029/2005jd005901, 2005.

Menon, S., Hansen, J., Nazarenko, L., and Luo, Y.F.: Climate effects of black carbon aerosols in China and India, Science, 297, 2250-2253, doi:10.1126/science.1075159, 2002.

Mikkonen, S., Romakkaniemi, S., Smith, J. N., Korhonen, H., Petäjä, T., Plass-Duelmer, C., Boy, M., McMurry, P. H., Lehtinen, K. E. J., Joutsensaari, J., Hamed, A., Mauldin III, R. L., Birmili, W., Spindler, G., Arnold, F., Kulmala, M., and Laaksonen, A.: A statistical proxy for sulphuric acid concentration. Atmos. Chem. Phys., 11, 11319-11334, doi:10.5194/acp-11-11319-2011, 2011.

Nie, W., Ding, A. J., Xie, Y.N., Xu, Z., Mao, H., Kerminen, V.-M., Zheng L.F., Qi, X.M., Yang, X.Q., Sun, J.N., Herrmann, E., Petäjä, T., Kulmala, M., and Fu, C.B.: Influence of biomass burning plumes on HONO chemistry in eastern China, Atmos. Chem. Phys., 15, 1147-1159, doi:10.5194/acp-15-1147-2015, 2015.

Nie, W., Ding, A.J., Wang, T., Kerminen, V.-M., George,C., Xue, L.K., Wang, W.X., Zhang, Q.Z., Petäjä, T., Qi, X.M., Gao, X.M., Wang, X.F., Yang, X.Q., Fu, C.B., Kulmala, M.: Polluted dust promotes new particle formation and growth, Scientific Reports, 4, 6634, doi:10.1038/srep06634, 2014.

Nieminen, T., Asmi, A., Dal Maso, M., Aalto, P. P., Keronen, P.,Petäjä, T., Kulmala, M., and Kerminen, V.-M.: Trends in atmospheric new-particle formation: 16 years of observations in a boreal-forest environment, Boreal Env. Res., 19, 191-214,2014.

Peng, J.F., Hu, M., Wang, Z.B., Huang, X.F., Kumar, P., Wu, Z.J., Guo, S., Yue, D.L., Shang, D.J., Zheng, Z., and He, L.Y.: Submicron aerosols at thirteen diversified sites in China: size distribution, new particle formation and corresponding contribution to cloud condensation nuclei production, Atmos. Chem. Phys., 14, 10249-10265, doi:10.5194/acp-14-10249-2014，2014.

Pope, C.A., Burnett, R.T., Thun, M.J., Calle, E.E., Krewski, D., Ito, K., and Thurston, G.D.: Lung cancer, cardiopulmonary mortality, and long term exposure to fine particulate air pollution, JAMA-J. Am. Med. Assoc., 287, 1132-1141, doi:10.1001/jama.287.9.1132, 2002.

Qian, Y., Leung, L.R., Ghan, S.J., and Giorgi, F.: Regional climate effects of aerosols over China: modeling and observation, Tellus Ser. B-Chem. Phys. Meteorol., 55, 914-934, doi:10.1046/j.1435-6935.2003.00070.x,2003.

Raes, f., Van Dingenen, R.,Vignati, E., Wilson, J., Putaud, J.-P., Seinfeld, J. H., and Adams, P.: Formation and cycling of aerosols in the global troposphere, Atmos. Environ., 34, 4215-4240, doi:10.1016/S1352-2310(00)00239-9, 2000.

Rao, S., Chirkov, V., Dentener, F., Van Dingenen, R., Pachauri, S., Purohit, P., Amann, M.,Heyes, C., Kinney, P., Kolp, P.,Klimont, Z., Riahi, K., and Schoepp, W.: Environmental modeling and methods for estimation of the global health impacts of air pollution, Environ. Model. Assess., 17, 613-622, doi:10.1007/s10666-012-9317-3, 2012.

Reid, J. S., Koppmann, R., Eck, T. F., and Eleuterio, D. P.: A review of biomass burning emissions

part II: intensive physical properties of biomass burning particles, Atmos. Chem. Phys., 5, 799-825, 2005.

Rose, C., Sellegri, K., Velarde, F., Moreno, I., Ramonet, M., Weinhold, K., Krejci, R., Andrade, M., Wiedensohler, A. and Laj, P.: Frequent nucleation events at the high altitude station of Chacaltaya (5240 m a.s.l.), Bolivia, Atmos. Environ., 102, 18–29, doi:10.1016/j.atmosenv.2014.11.015, 2015.

Shen, X. J. Sun, J. Y., Zhang, Y. M., Wehner, B., Nowak, A., Tuch, T., Zhang, X. C., Wang. T. T., Zhou, H. G., Zhang, X. L., Dong, F., Birmili, W., and Wiedensohler, A.: First long-term study of particle number size distributions and new particle formation events of regional aerosol in the North China Plain, Atmos. Chem. Phys., 11, 1565-1580, doi:10.5194/acp-11-1565-2011,2011.

Sihto, S.-L., Mikkilä, J., Vanhanen, J., Ehn, M., Liao, L., Lehtipalo, K., Aalto, P. P., Duplissy, J., Petäjä, T., Kerminen, V.-M., Boy, M., and Kulmala, M.: Seasonal variation of CCN concentrations and aerosol activation properties in boreal forest, Atmos. Chem. Phys., 11, 13269-13285, doi:10.5194/acp-11-13269-2011,2011.

Stanier, C. O., Khlysyov, A. Y., and Pandis, S. N.: Ambient aerosol size distributions and number concentrations measured during the Pittsburgh Air Quality Study (PAQS), Atmos. Environ., 38, 3275-3284, doi:10.1016/j.atmosenv.2004.03.020, 2004.

Tie, X.X., and Cao, J.J.: Aerosol pollution in China: Present and future impact on environment, Particuology, 7, 426-431, doi:10.1016/j.partic.2009.09.003,2009.

Tunved P., Hansson H.-C., Kerminen V.-M., Ström J., Dal Maso M., Lihavainen H., Viisanen Y., Aalto P. P., Komppula M. and Kulmala M.: High natural aerosol loading over boreal forests. Science 312, 261-263, 2006.

Tunved P., Nilsson E.D., Hansson H.-C. & Strom J.: Aerosol characteristics of air masses in northern Europe: influences of location, transport, sinks, and sources. J. Geophys. Res., 110, D07201, doi:10.1029/2004JD0005085, 2005.

Vakkari, V., Beukes, J.P., Laakso, H., Mabaso, D., Pienaar, J.J., Kulmala, M.,andLaakso, L.: Long-term observations of aerosol size distributions in semi-clean and polluted savannah in South Africa, Atmos. Chem. Phys., 13, 1751-1770, doi:10.5194/acp-13-1751-2013,2013.

Vakkari, V., Kerminen, V.-M., Beukes, J.P., Titta, P., van Zyl, P.G., Josipovic, M., Venter, A.D., Laars, K., Worsnop, D.R., Kulmala, M., and Laakso L.: Rapid changes in biomass burning aerosols by atmospheric oxidation, Geophys. Res. Lett., 41, 2644-2651, doi:10.1002/2014gl059396, 2014.

Wang, H.L., Zhu, B., Shen, L.J., An, J.L., Yin, Y., and Kang, H.Q.: Number size distribution of aerosols at Mt. Huang and Nanjing in the Yangtze River Delta, China: Effects of air masses and characteristics of new particle formation, Atmos. Res., 150, 42-56, doi:10.1016/j.atmosres.2014.07.020, 2014.

Wang, Y.G., Hopke, P.K., Chalupa, D.C., and Utell, M.J.: Long-term study of urban ultrafine particles and other pollutants, Atmos. Environ., 45, 7672-7680, doi:10.1016/j.atmosenv.2010.08.022, 2011.

Wehner, B., Birmili, W., Ditas, F., Wu, Z., Hu, M., Liu, X., Mao, J., Sugimoto, N., and Wiedensohler, A.: Relationships between submicrometer particulate air pollution and air mass history in Beijing, China, 2004-2006, Atmos. Chem. Phys., 8, 6155-6168, 2008.

Wiedensohler, A., Cheng, Y. F., Nowak, A., Wehner, B., Achtert, P., Berghof, M., Birmili, W., Wu, Z. J., Hu, M., Zhu, T., Takegawa, N., Kita, K., Kondo, Y., Lou, S. R., Hofzumahaus, A., Holland,

F., Wahner, A., Gunthe, S. S., Rose, D., Su, H.,andPöschl, U.: Rapid aerosol particle growth and increase of cloud condensation nucleus activity by secondary aerosol formation and condensation: A case study for regional air pollution in northeastern China, J. Geophys. Res., 114, D00G08, doi:10.1029/2008jd010884, 2009.

Wiedensohler, A.,Birmili, W., Nowak, A., Sonntag, A.,Weinhold, K., Merkel, M.,Wehner, B.,Tuch, T., Pfeifer, S.,Fiebig, M.,Fjaraa, A. M.,Asmi, E.,Sellegri, K.,Depuy, R.,Venzac, H.,Villani, P.,Laj, P., Aalto, P.,Ogren, J. A.,Swietlicki, E., Williams, P.,Roldin, P.,Quincey, P.,Huglin, C.,Fierz-Schmidhauser, R.,Gysel, M.,Weingartner, E.,Riccobono, F., Santos, S.,Gruning, C.,Faloon, K.,Beddows, D., Harrison, R. M., Monahan, C., Jennings, S. G., O'Dowd, C. D.,Marinoni, A., Horn, H. G., Keck, L., Jiang, J.,Scheckman, J.,McMurry, P. H., Deng, Z., Zhao, C. S.,Moerman, M.,Henzing, B., de Leeuw, G.,Loschau, G., and Bastian, S.: Mobility particle size spectrometers: harmonization of technical standards and data structure to facilitate high quality long-term observations of atmospheric particle number size distributions, Atmos. Meas. Tech., 5, 657-685,doi:10.5194/amt-5-657-2012, 2012

Woo, K.S., Chen, D.R., Pui, D.Y.H., and McMurry, P.H.: Measurement of Atlanta aerosol size distributions: Observations of ultrafine particle events, Aerosol Sci. Technol., 34, 75-87, doi:10.1080/027868201300082049, 2001.

Wu, Y.-X., Yin, Y., Gu, X.-S, and Tan, H.-B.: An observational study of the hygroscopic properties of aerosols in north suburb of Nanjing, China Environmental Science, 34(8), 1938-1949, 2014.

Wu, Z. J., Hu, M., Liu, S., Wehner, B., Bauer, S., Ssling, A. M., Wiedensohler, A., Petäjä, T., Dal Maso, M., and Kulmala, M.: New particle formation in Beijing, China: Statistical analysis of a 1-year data set, J. Geophys. Res., 112, D09209, doi:10.1029/2006jd007406, 2007.

Wu, Z. J., Hu, M., Lin, P., Liu, S., Wehner, B., and Wiedensohler, A.: Particle number size distribution in the urban atmosphere of Beijing, China, Atmos. Environ., 42, 7967-7980, doi:10.1016/j.atmosenv.2008.06.022, 2008.

Yli-Juuti, T., Riipinen, I., Aalto, P.P., Nieminen, T., Ugent, W.M., Janssens, I.A., Claeys, M., Salma, I., Ocskay, R., Hoffer, A., Imre, K., and Kulmala, M.: Characteristics of new particle formation events and cluster ions at K-Puszta, Hungry, Boreal Environ. Res., 14, 683-698, 2009.

Young, L.-H., Benson, D. R., Montanaro, W. M., Lee, S.-H., Pan, L. L., Rogers, D. C., Jensen, J., Stith, J. L., Davis, C. A., Campos, T. L., Bowman, K. P., Cooper, W. A. and Lait, L. R.: Enhanced new particle formation observed in the northern midlatitude tropopause region, J. Geophys. Res. Atmospheres, 112(D10), D10218, doi:10.1029/2006JD008109, 2007.

Zhang, Q., Jimenez, J. L., Canagaratna, M. R., Allan, J. D., Coe, H., Ulbrich, I., Alfarra, M. R., Takami, A., Middlebrook, A. M., Sun, Y. L., Dzepina, K., Dunlea, E., Docherty, K., DeCarlo, P. F., Salcedo, D., Onasch, T., Jayne, J. T., Miyoshi, T., Shimono, A., Hatakeyama, S., Takegawa, N., Kondo, Y., Schneider, J., Drewnick, F., Borrmann, S., Weimer, S., Demerjian, K., Williams, P., Bower, K., Bahreini, R., Cottrell, L., Griffin, R. J., Rautiainen, J., Sun, J. Y., Zhang, Y. M., and Worsnop, D. R.: Ubiquity and dominance of oxygenated species in organic aerosols in anthropogenically-influenced Northern Hemisphere multitudes, Geophys. Res. Lett., 34, L13801, doi:10.1029/2007GL029979, 2007.

Zhang, Q., Streets, D. G., Carmichael, G. R., He, K. B., Huo, H.,Kannari, A., Klimont, Z., Park, I. S., Reddy, S., Fu, J. S., Chen, D., Duan, L., Lei, Y., Wang, L. T., and Yao, Z. L.: Asian emissions in 2006 for the NASA INTEX-B mission, Atmos. Chem. Phys., 9,5131-5153, doi:

10.5194/acp-9-5131-2009, 2009.

Appendix: Performance of the flow-switching DMPS

The flow-switching DMPS has two flow modes to measure the particles in two size ranges, 6-100 nm and 100-800 nm, respectively. To assimilate data in the two flow modes, in this study the number concentrations of particles in the size range from 100 to 800 nm were multiplied by a factor to make the particle number size distribution smooth. The correction was done for daily data. The average correction factor was 1.05±0.11, which means that in this size range the original inverted number concentrations increased on the average by 5%. The 10th, 25th, 50th, 75th and 90th percentiles of this correction factor were 0.92, 0.96, 1, 1.1 and 1.2, respectively.

The model of CPC used in this study was the TSI 3772 with the 10 nm default cut-off diameter when the condenser temperature is at the default value of 22 ^{o}C. It was set to 10°C in this measurement, so the temperature difference ΔT between the saturator and the condenser was higher (ΔT>25 ^{o}C) which leads to a higher supersaturation and a lower cut-off diameter. The counting efficiency of 6nm particles is higher than 75% (Wiedensohler et al., 2012).

The DMPS was set up so that every time before number size distribution measurement, the DMA was by-passed, and total aerosol number concentration was determined directly by the CPC (Yli-Juuti et al., 2009). The average ratio of the total particle number concentration of that integrated from the inverted size distributions and measured directly with the CPC (N_{DMPS} and N_{CPC}) was 0.90±0.17 and the correlation coefficient was 0.91 ($p<1*10^{-6}$). The 10th, 25th, 50th, 75th and 90th percentiles were 0.71, 0.82, 0.91, 0.99 and 1.06, respectively. These values can indicate that data quality of the DMPS was satisfactory.

Figure S1 shows the scatter plot of N_{DMPS} and N_{CPC} color-coded with the arithmetic mean diameter of the whole particle number size distribution ($AMD_{6\text{-}800\ nm}$). The ratio of N_{DMPS} to N_{CPC} was low when the $AMD_{6\text{-}800\ nm}$ was small but close to 1 when the $AMD_{6\text{-}800\ nm}$ was large. As the small $AMD_{6\text{-}800\ nm}$ corresponds to new particle formation events with a high concentration of nucleation mode particles, the lower N_{DMPS}-to-N_{CPC} ratio suggests that the DMPS (including the inversion) may have underestimated the concentration of them. This is in line with the inter-comparison study presented by Wiedensohler et al. (2012) where it was found that the largest uncertainties of the size distributions were in the nucleation mode.

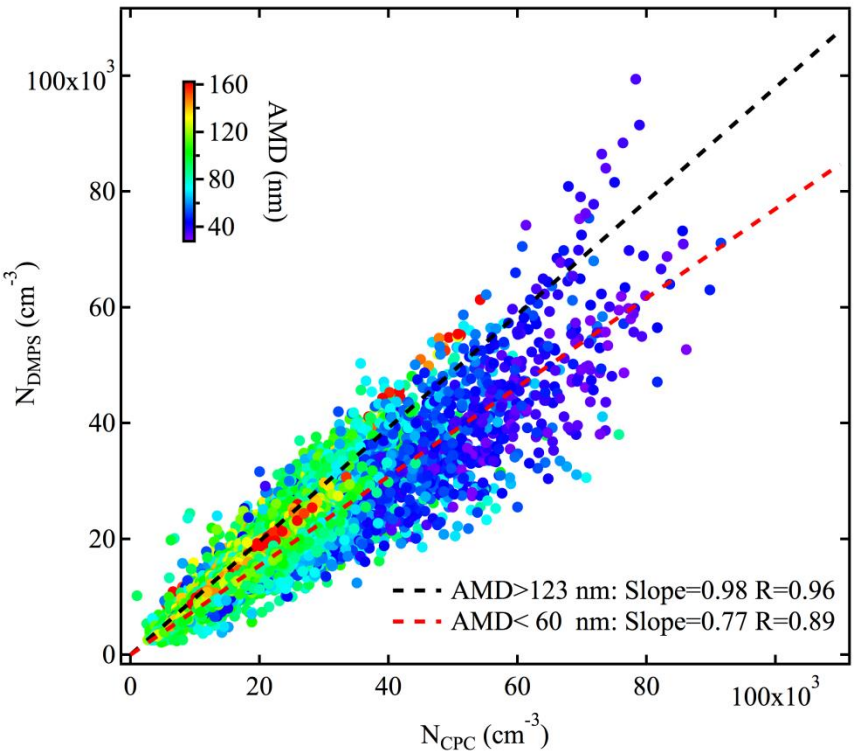

Figure S1 The scatter plot of N_{DMPS} vs. N_{CPC} color-coded with the arithmetic mean diameter of the particle number size distribution ($AMD_{6\text{-}800\ nm}$). Note: Linear fits for the data when the $AMD_{6\text{-}800\ nm}$ is higher than 123nm (90th percentiles of the $AMD_{6\text{-}800\ nm}$ distribution) or lower than 60nm (10th percentiles of the $AMD_{6\text{-}800\ nm}$ distribution) are shown in the figure.

Figures and Tables

Table 1. Overall statistics for the number concentrations and relevant parameters calculated based on DMPS measurement at the SORPES site during December 2011–November 2013.

	Annual	Spring	Summer	Autumn	Winter
Total particles (cm^{-3})	19200[A] ±9200[B]	20600 ±9000	18000 ±10800	18000 ±7600	19900 ±9300
Nucleation mode(cm^{-3})	5300 ±5500	6200 ±5900	4600 ±5500	4800 ±4900	5700 ±5400
Aitken mode (cm^{-3})	8000 ±4400	8500 ±4000	8100 ±5700	7600 ±3900	7800 ±3900
Accumulation mode(cm^{-3})	5800 ±3200	5900 ±2900	5300 ±4200	5600 ±2500	6500 ±3000
$AMD_{6\text{-}800\ nm}$ (nm)	92 ±25	89 ±23	90 ±26	92 ±26	97 ±26
CS ($10^{-2}\ s^{-1}$)	3.8 ±2.0	4.0 ±1.7	3.5 ±2.5	3.6 ±1.7	4.2 ±1.9
CS_{wet} ($10^{-2}\ s^{-1}$)	5.3 ±2.9	5.5 ±2.6	5.0 ±3.7	5.1 ±2.7	5.8 ±2.7

A: Mean, B: Standard deviation, $AMD_{6\text{-}800\ nm}$: Arithmetic Mean Diameter of 6–800 nm particles, CS: Condensation sink

CS_{wet}: Condensation sink with the consideration of hygroscopic growth

Table 2. Statistics of NPF events, J_6, $GR_{6\text{-}30\ nm}$ and CS at the SORPES station during the two-year measurement period

		Spring	Summer	Autumn	Winter
Event Classification	Class I	52	44	64	10
	Class II	42	29	24	5
	Non-event	75	60	89	115
	Undefined	3	3	1	4
J_6 ($cm^{-3}s^{-1}$)	Mean ±SD	3.6 ±2.4	2.1 ±1.4	2.1 ±1.9	1.8 ±1.6
$GR_{6\text{-}30\ nm}$(nm/h)	Mean ±SD	10.0 ±3.4	12.8 ±4.4	8.9 ±2.9	9.5 ±3.3

Table 3. Statistics of NPF events in different air masses backward trajectories of clusters.

	Class I	**Class II**	**Non-event**	**Undefined**
C1	52	25	82	3
C2	25	19	48	0
C3	32	22	12	0
C4	33	13	69	4
C5	20	11	72	3

Table 4. Correlation coefficients of J_6 and $GR_{6\text{-}30\ nm}$ with main meteorological parameters and air pollutants

	Temp (^oC)	RH (%)	Rad (W/m^2)	O_3 (ppbv)	$PM_{2.5}$ ($\mu g/m^3$)	SO_2 (ppbv)	NO_x (ppbv)	CS ($10^{-2}s^{-1}$)
J_6 ($cm^{-3}s^{-1}$)	0.10	-0.31*	0.32*	0.17*	0.01	0.11	-0.01	0.06
$GR_{6\text{-}30\ nm}$ (nm/h)	0.36*	0.27*	0.27*	0.38*	0.07	0.06	-0.14	0.38*

*: The correlation coefficient passes the statistical significant test ($p<0.05$).

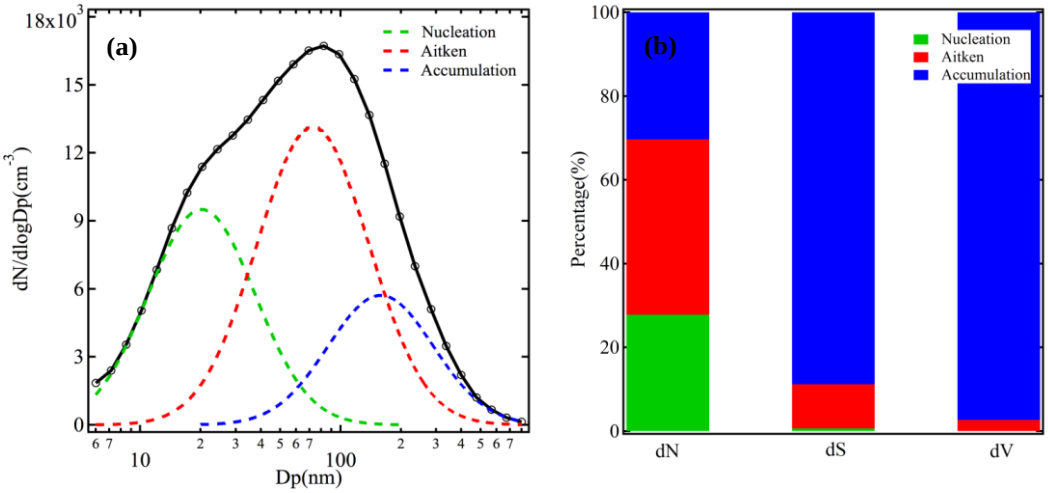

Fig. 1. (a) Averaged number size distribution and lognormal fitting curves of three modes, and **(b)** averaged fraction of the particles number, surface and volume concentrations in the three modes measured at the SORPES site during December 2011–November 2013.

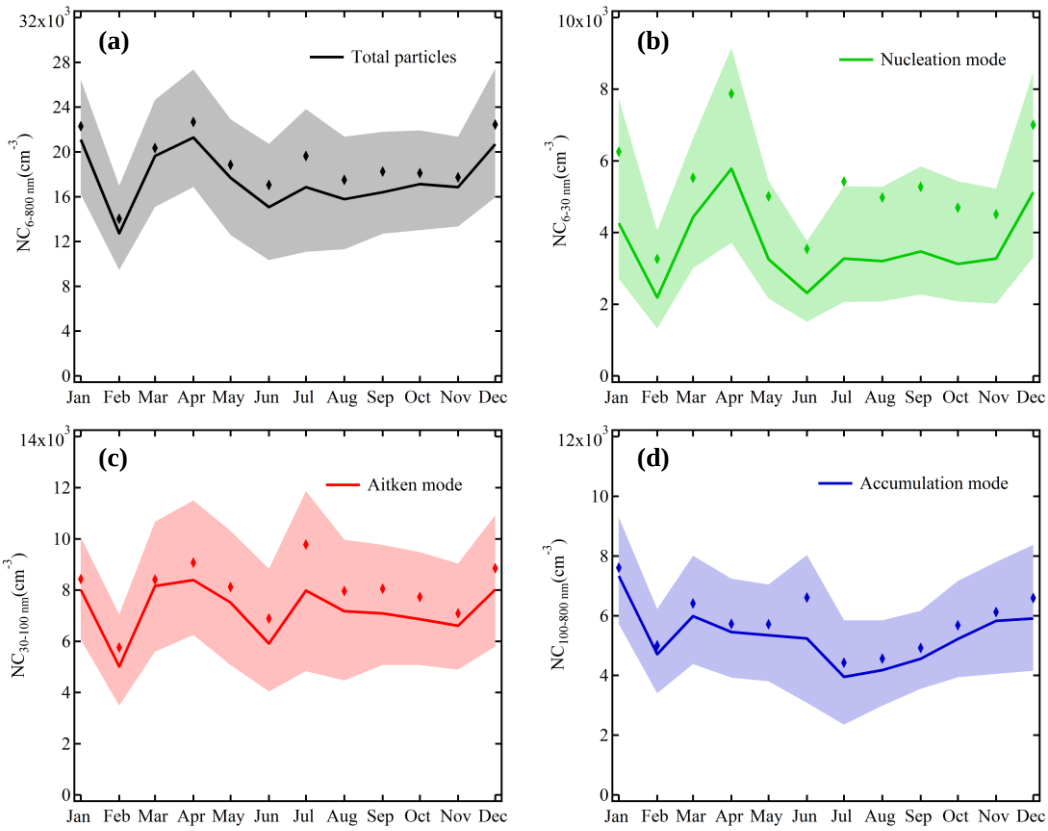

Fig. 2. The averaged seasonal variations of **(a)** the total particle number concentration and number concentrations in the **(b)** nucleation, **(c)** Aitken and **(d)** accumulation mode. Note: Bold solid lines are the monthly median and shaded area represents the 25th or 75th percentiles. The diamond markers represent the monthly average.

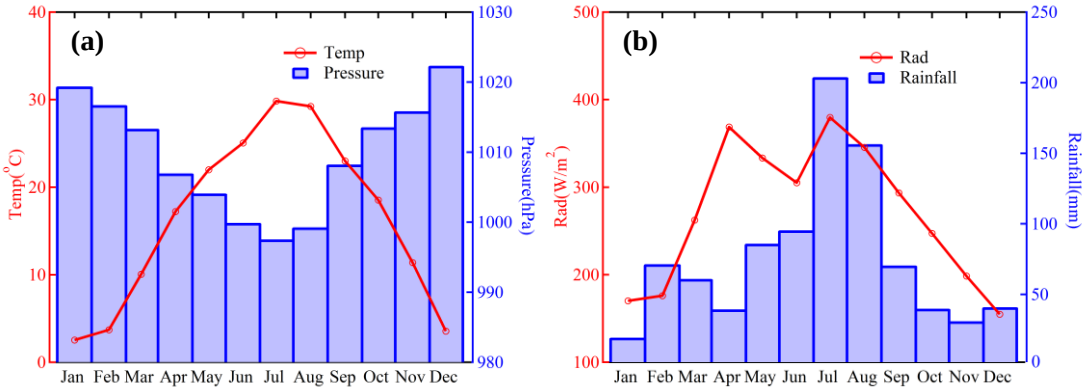

Fig. 3. Averaged seasonal variations of **(a)** temperature and pressure, **(b)** radiation and rainfall during the entire measurement period.

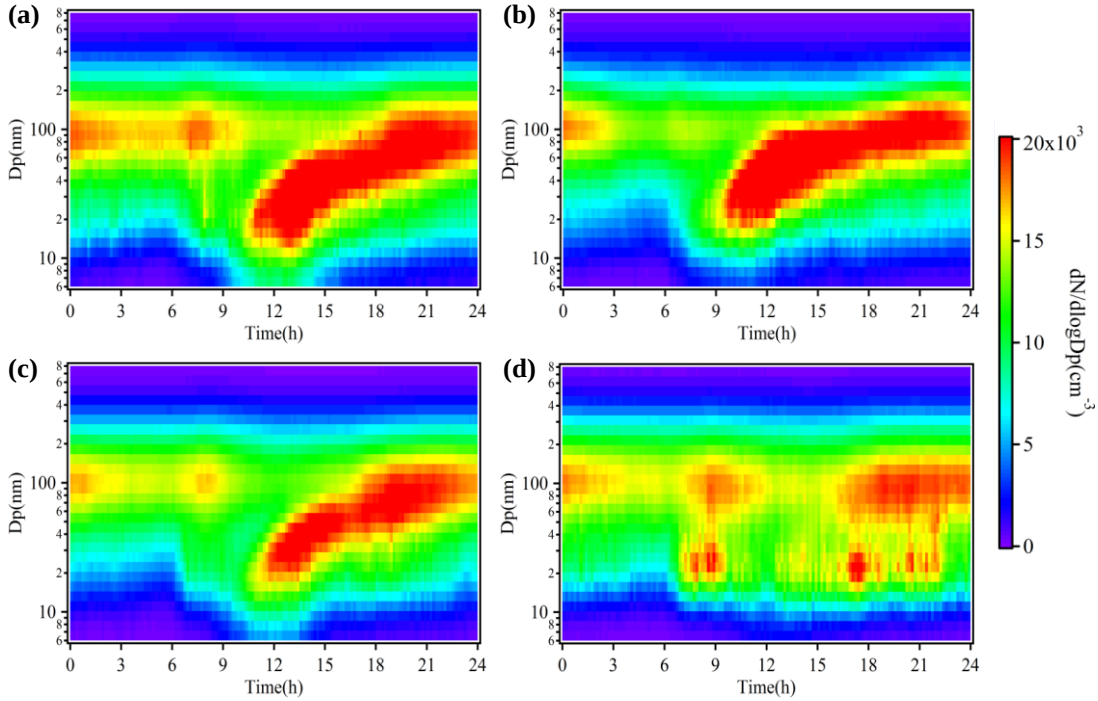

Fig. 4. Averaged diurnal cycles of particle number size distributions for **(a)** spring, **(b)** summer, **(c)** autumn and **(d)** winter at the SORPES station during the 2-year measurement period.

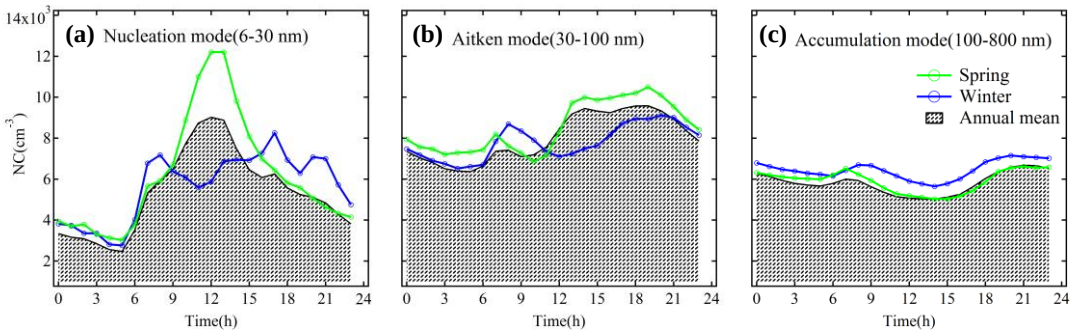

Fig. 5. Averaged diurnal variations of particle number concentrations in **(a)** Nucleation mode, **(b)** Aitken mode, **(c)** accumulation mode in spring, winter and entire period during the two-year measurement period.

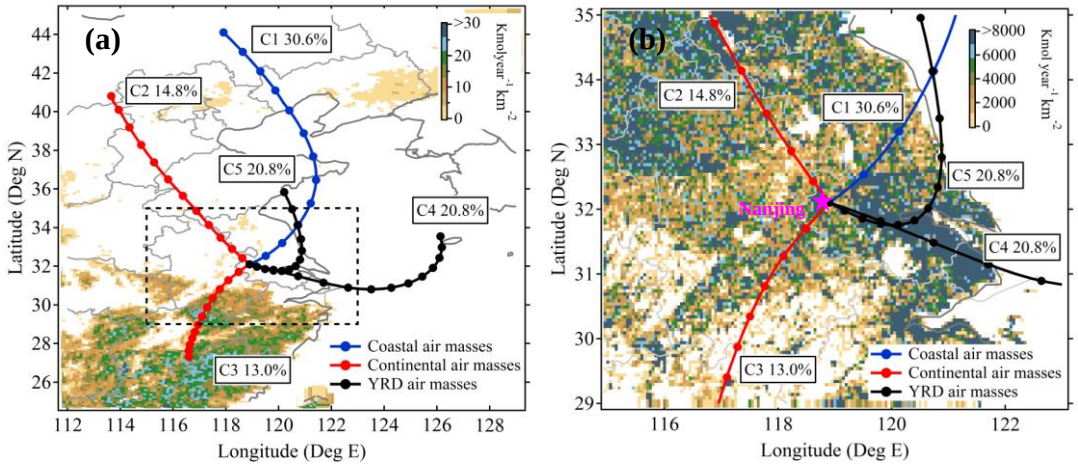

Fig. 6. Mean air mass backward trajectories of five clusters showing on map of **(a)** monoterpene in East China and **(b)** anthropogenic VOCs in the YRD. Note: Points of trajectories represent the six-hourly location. The percentages of each cluster are tabulated in the map. The monoterpene data were calculated by MEGAN (Model of Emissions of Gases and Aerosols from Nature) with MM5(the Fifth-Gneration Mesoscale Model) providing meteorological data and the anthropogenic VOCs data were accessed from MEIC (Multi-resolution Emission Inventory for China) database (http://www.meicmodel.org/).

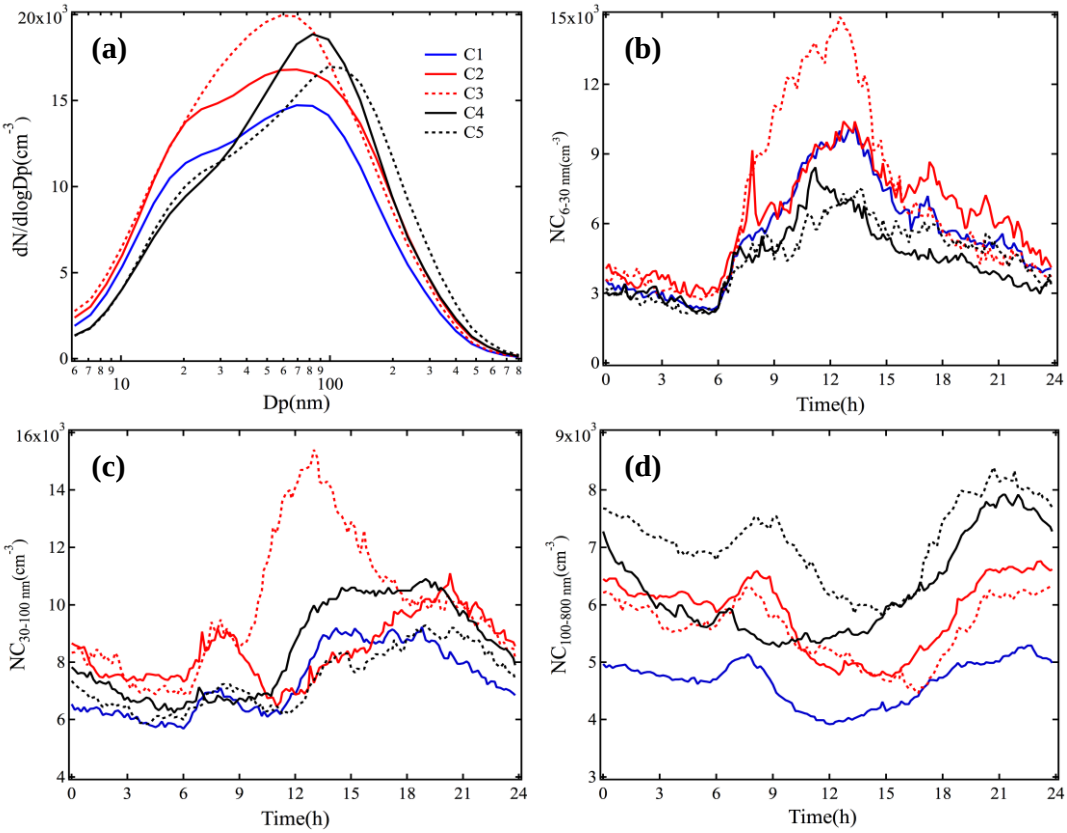

Fig. 7. (a) Particles number size distributions of five clusters (C1, C2, C3, C4 and C5 air masses, respectively); Diurnal variations of particle number concentration of five clusters in **(b)** nucleation (6-30 nm), **(c)** Aitken (30-100 nm) and **(d)** accumulation mode (100-800 nm).

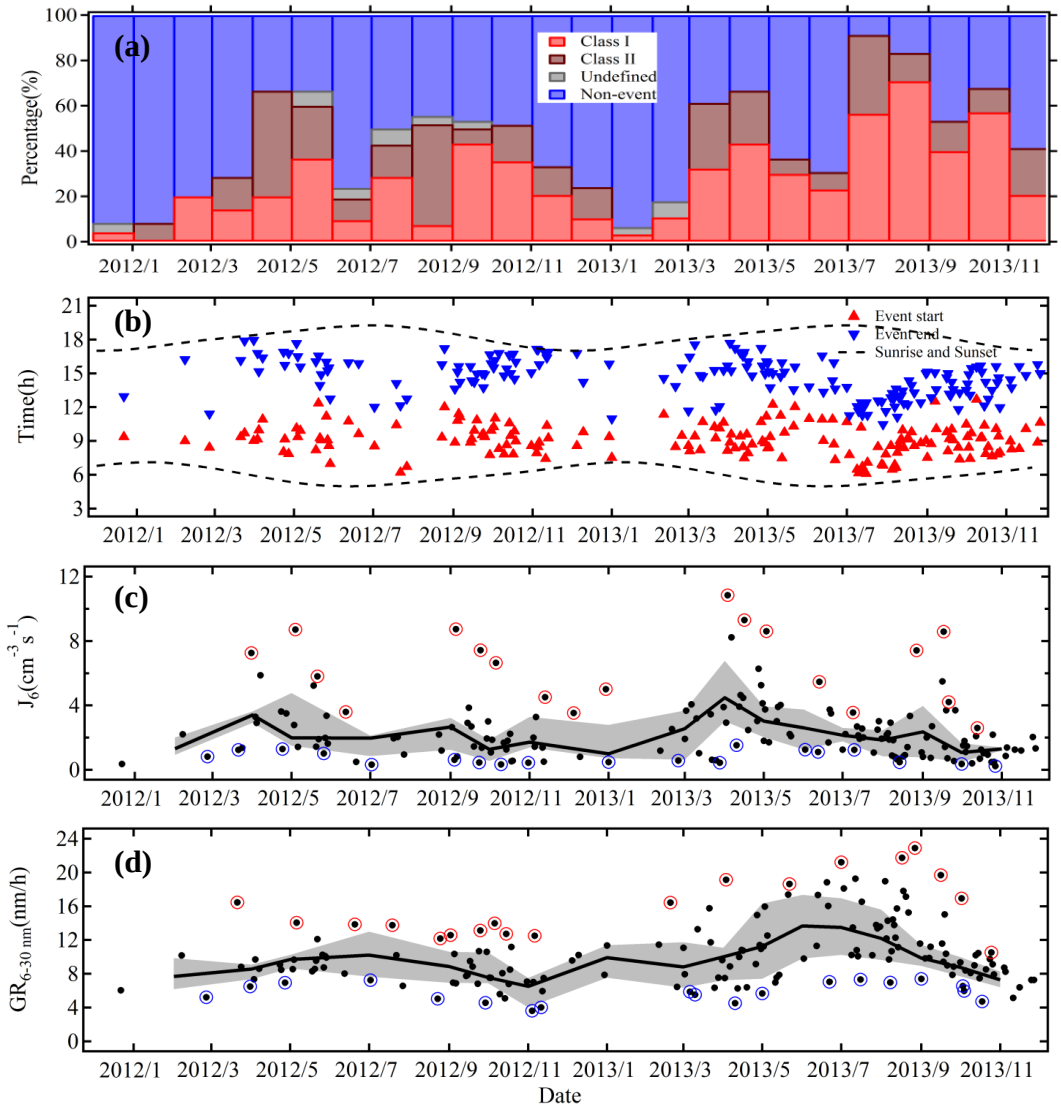

Fig. 8. Monthly time series of **(a)** the fraction of Class I, Class II NPF events, undefined and non-event days, **(b)** start time and end time of Class I event days, **(c** and **d)** J_6 and growth rate during Class I event days. Note: Dashed lines in Fig. 8b represent the sunrise and sunset time. Bold solid lines in Fig. 8c and 8d are the median values and shaded area represents the 25th or 75th percentiles. Red circles and blue circles in Fig. 8c and 8d are the days that selected for further investigation in Sect. 3.2.3.

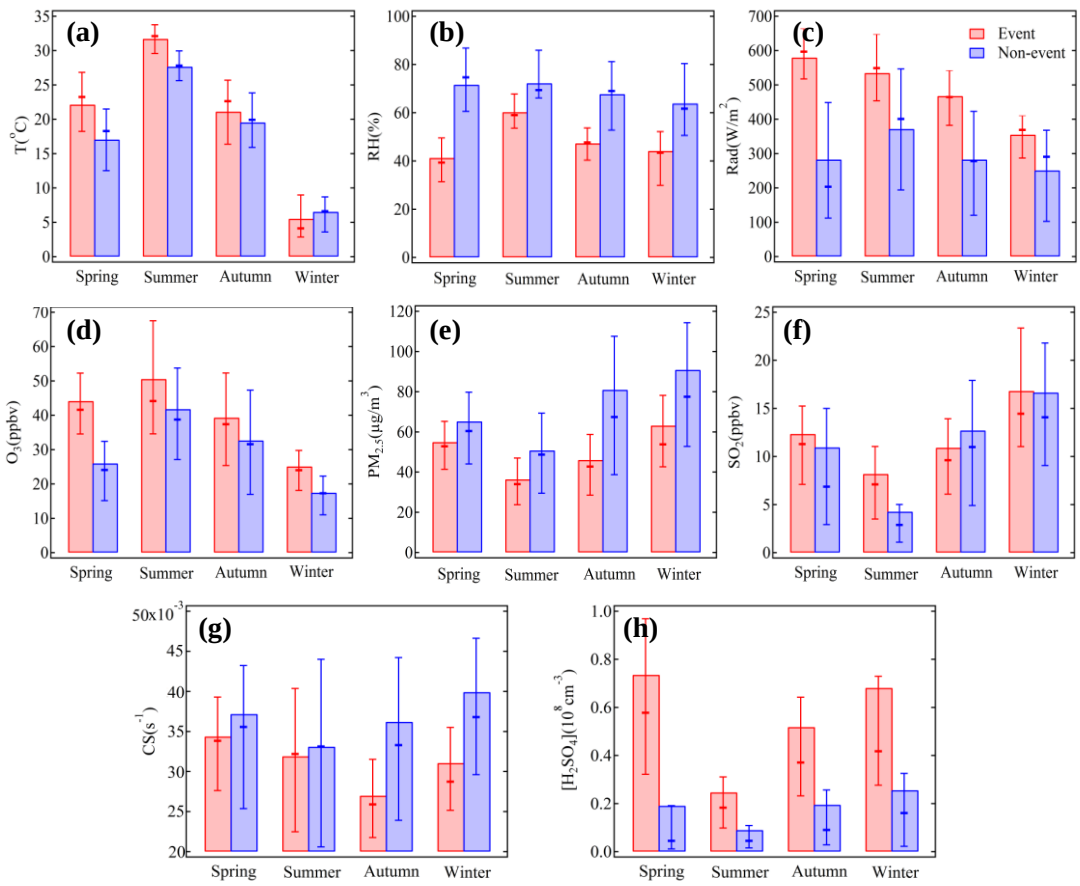

Fig. 9. (a-c) Meteorological variables, **(d-f)** gaseous pollutants, **(g)** condensation sink and **(h)** H_2SO_4 proxy during event (Red) and non-event (Blue) days in different seasons. Note: Bars are the mean value. The bold stick and whiskers are median values and 25th or 75th percentiles.

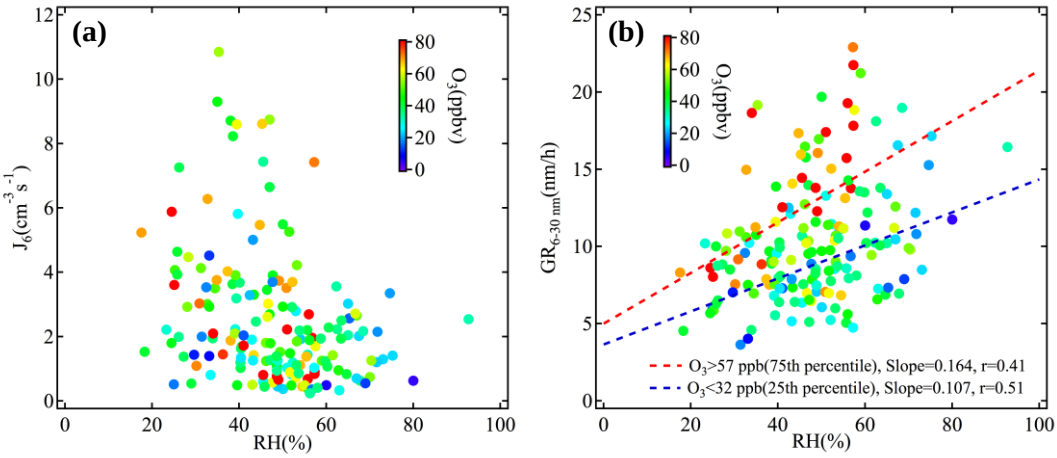

Fig. 10. Scatter plot **(a)** between J_6 and RH and **(b)** between $GR_{6\text{-}30\ nm}$ and RH, color-coded with the O_3 concentration. Note: Linear fits for the data when the O_3 concentration is higher than 57 ppbv (the 75th percentile) or lower than 32 ppbv (the 25th percentile) are shown in Fig. 10b, respectively.

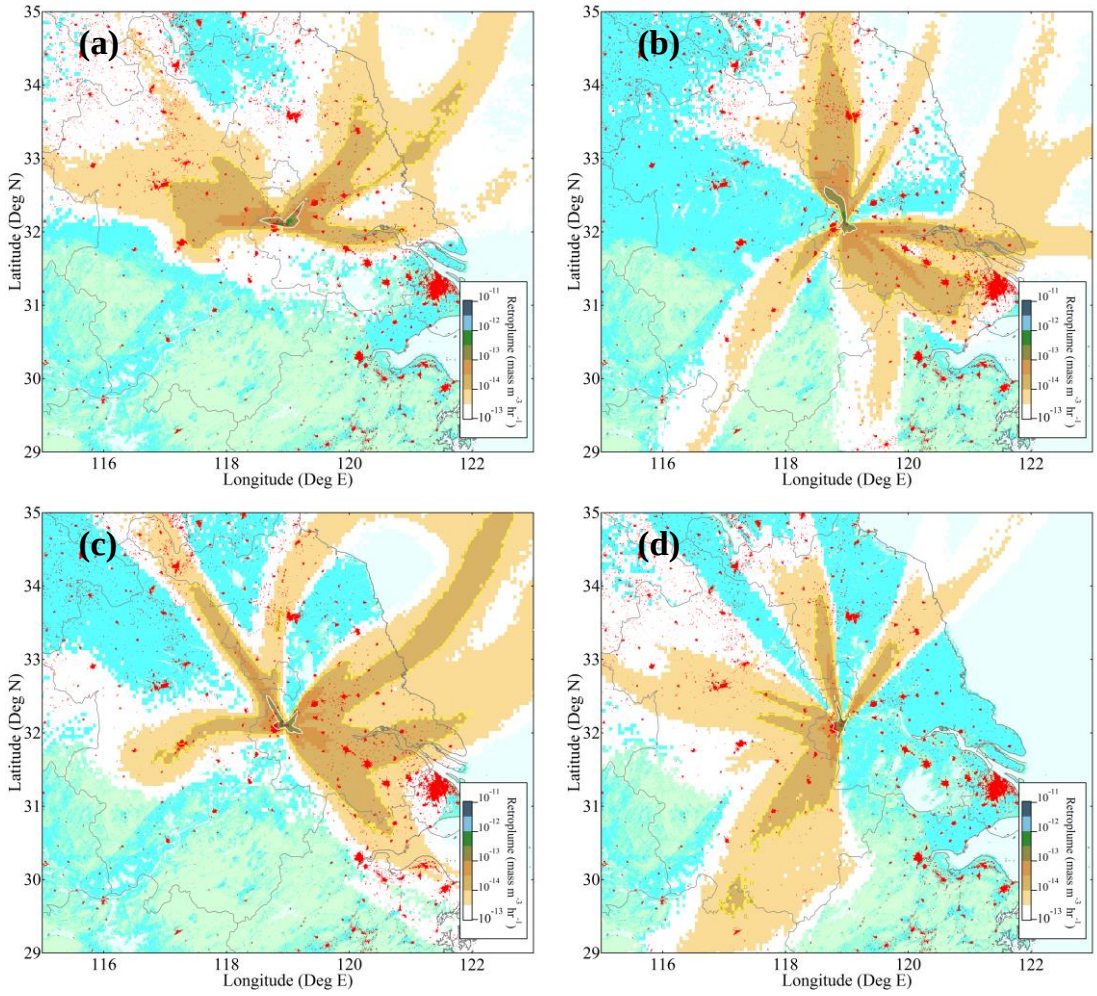

Fig. 11. The averaged retroplumes (i.e. 100 m footprint) of the selected events: **(a)** high J_6, **(b)** low J_6, **(c)** high GR, **(d)** low GR days. Note: Red area in the maps shows the location and size of city.

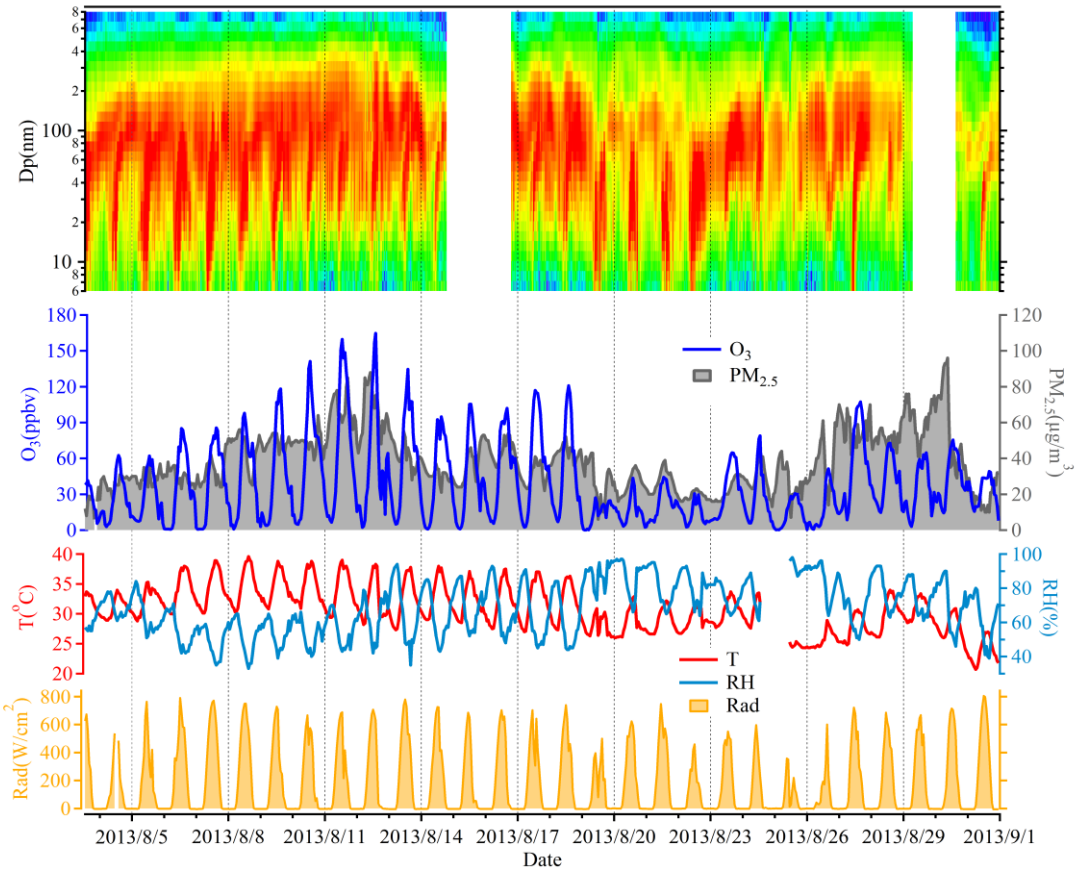

Fig. 12. Time series of **(a)** particles number size distribution, **(b)** O_3 and $PM_{2.5}$ concentrations, **(c)** temperature and RH, and **(d)** intensity of radiation measured at SORPES site in August 2013.

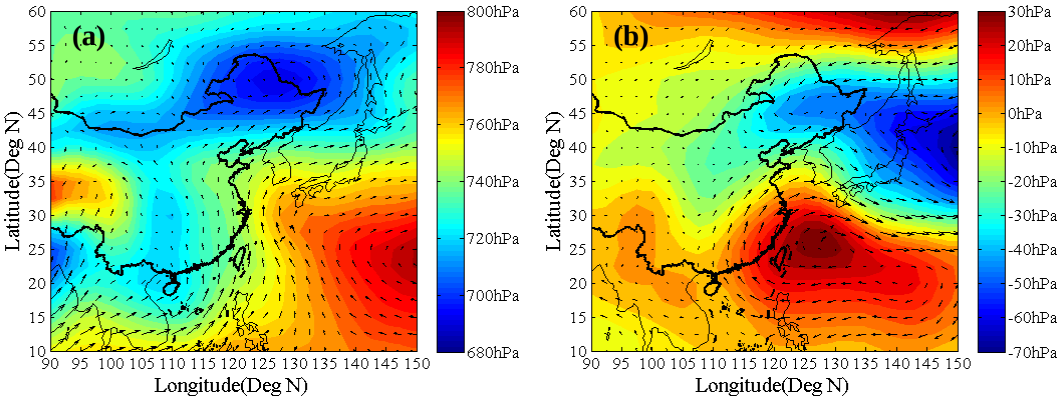

Fig. 13. (a) Average geopotential height and wind vector at the 925-hPa level during August 2013. **(b)** Differences in geopotential height and wind vector between Aug 2013 and Aug 2012 at the 925-hPa level.

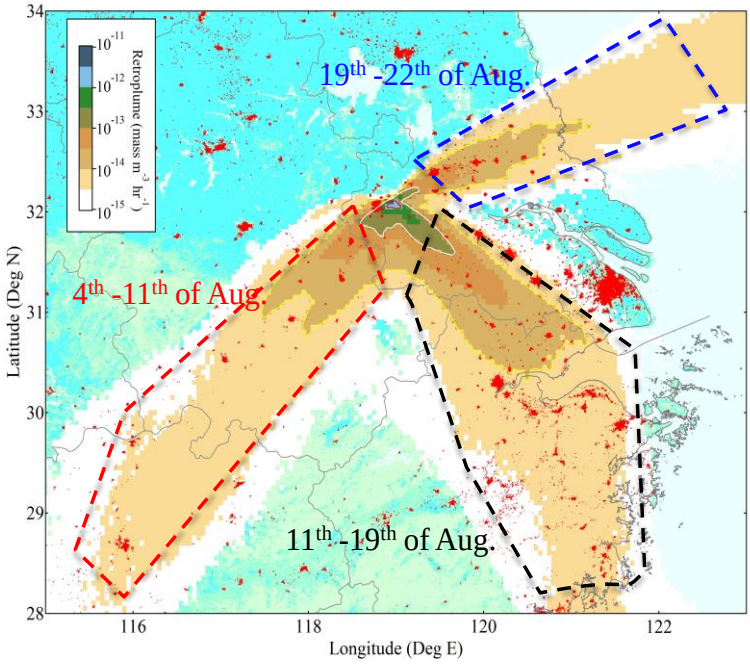

Fig. 14. Retroplumes from 4 to 22 August 2013 identified with three main periods. Note: Red points denote the urban area.

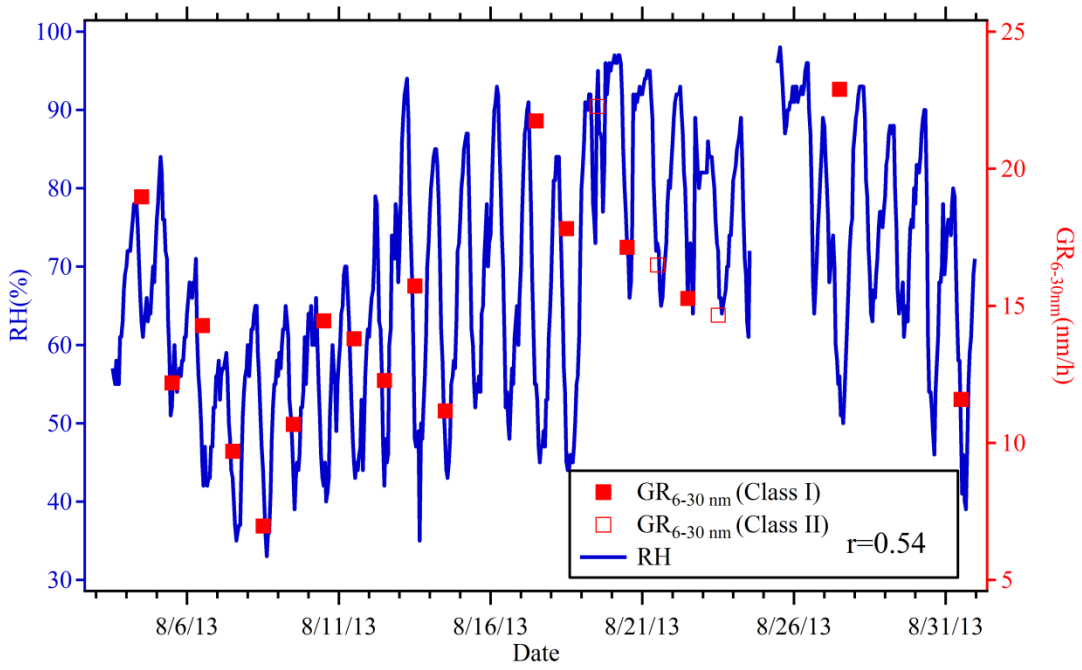

Fig. 15. Time series of RH and the $GR_{6\text{-}30\ nm}$ of NPF days (Class I and Class II) in August 2013